Chapter 7
Curvilinear Magnetic Architectures for Biomedical Engineering

Larysa Baraban, Tao Huang, Xiangzhong Chen, Ramon Santiago Herrera Restrepo, Jordi Ignés Mullol, Josep Puigmartí-Luis, and Salvador Pané

Abstract The field of autonomous motile micro/nanomotors that can propel in the liquid environment strongly benefits from the use of magnetic materials, winning in the long-time deterministic locomotion and controllability of such microscopic objects. This chapter reviews the applications of curved magnetic micro/nanostructures to be employed for biomedical and environmental applications. In this respect, after introducing the basic principle and examples of the self-propelled micro-objects, we further focus here on the locomotion of the magnetically decorated microscopic objects and the influence of their shape on the character and pattern of the motion. Namely, we consider the properties of magnetically capped spherical Janus particles, rod-like, tubular, and other asymmetric objects, e.g., microhelices, with

L. Baraban (✉) · T. Huang
Institute of Radiopharmaceutical Cancer Research, Helmholtz-Zentrum Dresden-Rossendorf e.V., 01328 Dresden, Germany
e-mail: l.baraban@hzdr.de

T. Huang
e-mail: t.huang@hzdr.de

X. Chen · S. Pané
Multi-Scale Robotics Lab (MSRL), Institute of Robotics and Intelligent Systems (IRIS), ETH Zurich, Zurich CH-8092, Switzerland
e-mail: chenxian@ethz.ch

S. Pané
e-mail: vidalp@ethz.ch

R. S. Herrera Restrepo · J. Ignés Mullol · J. Puigmartí-Luis
Departament de Ciència dels Materials i Química Fsica, Institut de Química Teórica I Computacional, Barcelona 08028, Spain
e-mail: rsherrera7@ub.edu

J. Ignés Mullol
e-mail: jignes@ub.edu

J. Puigmartí-Luis
e-mail: josep.puigmarti@ub.edu

D. Makarov and D. D. Sheka (eds.), *Curvilinear Micromagnetism*,
Topics in Applied Physics 146, https://doi.org/10.1007/978-3-031-09086-8_7

magnetic functionalization. Finally, we describe the applications of such magnetic objects in environmental remediation, biosensing and drug delivery, etc.

7.1 General Overview of the Field: Magnetic Micro/Nanomotors

Artificial micro/nanomotors [1–3] can replace the work of surgeons at the micro/nanometer scales, assist in drug delivery [4–11], and carry out various biochemical experiments, such as transport and manipulation of cells [12]. Speech of Richard Feynman "*There's plenty of room at the bottom*" [13] predicted and inspired the development of nanotechnology, which gave us the next generation of miniaturized devices, and predicted the emergence of small micro/nanomotors. At that time, it was clear that the realization of such ambitious goals was not possible without the invention of the new sophisticated processing tools and merging the efforts from multiple disciplines, e.g., physics, chemistry, materials science, biology, and medicine. This requirement was fulfilled over several decades by introducing micro/nanostructuring techniques, scanning electron, tunneling microscopy, etc. With the maturing of nanotechnology, the scientific community became fully equipped to realize Feynman's fantasy about the micro/nanomotors operating with, e.g., living cells and organoids [14]. The development of the micro/nanomotor is fast by now, and years of active research have resulted in several classes of artificial micro/nanomotors that can efficiently convert energy, e.g., light, chemical, and thermal, into mechanical movements in a liquid environment. These micro/nanodevices hold promises to be used in several applications, ranging from diagnosis and targeted drug delivery up to manipulation and isolation of cells, and nanosurgery in biomedicine, as well as environmental remediation [15, 16]. Diverse external stimuli, including chemical [17], acoustic [12, 18–20], electrical [21–23], optical [24–27], magnetic [28–31], or combinations of these, can be utilized to power micro/nanomotors (Fig. 7.1) [32–34]. For example, chemically powered micro/nanomotors use localized catalytic decomposition of fuel molecules (e.g., H_2O_2) dissolved in the aqueous solution, forming a concentration gradient around their surface, to generate net propulsion [15, 35]. The enzymes, for example, glucose oxidase [36], urease [37], catalase [36], can be coupled to the artificial components and provide motion to micro/nanoobjects by catalytic reaction. Light is used to activate chemical reactions to achieve movement of microparticles or to produce temperature gradients under near-infrared illumination. Finally, the acoustic propulsion or alternating current (AC) magnetic field is valid as fuel-free mechanisms that can operate even in pure water. Figure 7.1 summarizes these diverse propulsion mechanisms for micro/nanomotors.

Indeed, this diversity of micromotors is realizable, thanks to the broad range of materials used to predesign their properties on demand. On the one hand, semiconductor, transient metal, noble metal, reactive salts can be used as a backbone of the

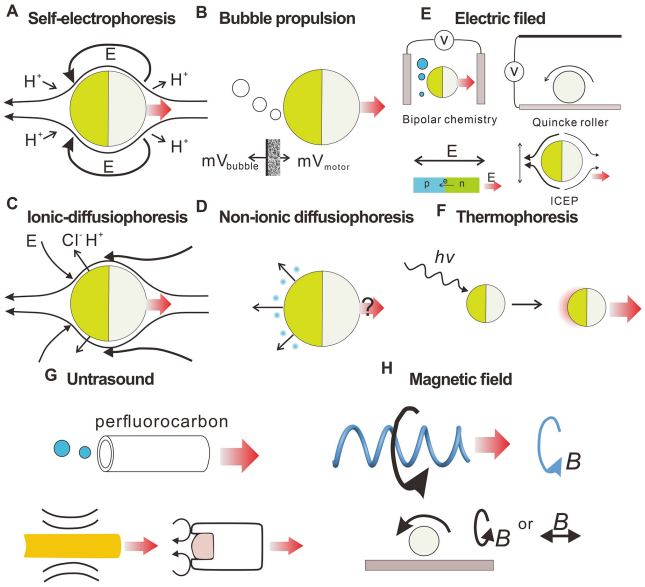

Fig. 7.1 Illustrations of diverse propulsion mechanisms of micro/nanomotors. **A** The self-electrophoretic locomotion of a motor requires a self-generated electric field and a charged motor surface. The electrochemical reactions occurring on the micro/nanomotor surface establish a proton concentration gradient and form a self-generated electric field, the electric field couples with charged micro/nanomotor and drive it moving forward. **B** Janus particle powered by asymmetrically decomposing fuel into a bubble; when a bubble detaches from the surface of a microparticle, its momentum is transferred to the particle and pushes it in the opposite direction. **C–D** Self-diffusiophoresis occurs when a colloidal particle generates a concentration gradient of a solute and moves in response to propulsive forces generated by that gradient. **C** Self-propulsion mainly arises from the diffusion of ionic chemical species. **D** Self-propulsion arises from gradients of electrically neutral solute molecules or particles. **E** DC electric field can induce chemical reactions that then cause motion via electrophoresis, diffusiophoresis, or bubble propulsion. DC electric fields can also induce an electrokinetic effect called Quincke rotation, leading to the rotation and movement of dielectric microspheres immersed in low conductivity liquids. In addition, a diode can rectify an alternating electric field and generate an electrokinetic flow, causing it to self-propel. Lastly, under AC electric fields, metal-dielectric Janus microparticle exhibits an asymmetric electroosmotic flow, which pushes the particle away from the metal hemisphere. **F** Heat powers colloidal motors by self-thermophoresis, which relies on an asymmetric distribution fluid temperature around a particle. **G** Ultrasound-powered motors, including an asymmetric microrod moving owing to local microstreaming, a microtube ejecting bubbles as perfluorocarbon vaporizes under ultrasound, and a microparticle moving away from an oscillating bubble trapped at a cavity. **H** A magnetic particle rolls near a surface in a rotating or oscillating magnetic field. Adapted with permission from [38].

motor or as a catalyst to initiate chemical propulsion and form a solute concentration gradient around micro/nanomotor. On the other hand, flexible building blocks can assemble together and mimic the bacterial flagella and move under a rotating magnetic field. Recent publications also suggest the use of biological components to fabricate biohybrid artificial micro/nanomotors or robots, e.g., actuators based on bacteria and other motile cells or actuators based on explanted whole-muscle tissue [39].

Over a decade, external fields have been considered an efficient mechanism to control and drive micro-objects via change of their spacetime symmetry in a liquid environment, staying as a non-invasive way of manipulation. This wireless actuation allows shapeable micro/nanomotors to move in an untethered manner, for example, spherical or rod-like motors, driven by chemical mechanisms—to reveal the deterministic motion pattern. Unlike the chemical or photochemical propulsion method, shapeable micro/nanomotor does not consume any fuel and only depends on the configuration and the symmetry of the objects [31]. Such systems implement magnetic thin films (from several nanometers up to a few micrometers thick) [40, 41], or explore magnetic nanoparticles to assure the ability of the motors to reorient when placed in an external magnetic field [42]. The advantages of such types of micromotors are intriguing: they are easy to fabricate, and the magnetic materials can be combined to customize their properties, as well as the shape of the object, which can be shaped to suit the application (e.g., spirals [43, 44], rods [45], tubes [46, 47]).

Magnetic micromotors can be classified into two subgroups (Fig. 7.2): (i) micromotors that do not require magnetic materials to create movement; instead, other mechanisms, e.g., chemical and optical, are used to create movement, and magnetic materials are only used to rectify the motion (panel A); and (ii) micromotors that do require magnetic materials to create motion, similar to non-reciprocal motility concepts (panel B).

While using microparticles (typical dimensions from one to several tens of micrometers), we consider their Brownian character of motion that involves both translational and rotational components. Efficient suppression of the last one would enable the rectified motion of the motors in a liquid environment. Here the proper selection of the object geometry and the materials themselves are critical for achieving the (a) motility and (b) deterministic motion pattern of the micromotors. For instance, multiple reports show the use of thin magnetic films with an in-plane easy axis of magnetization (e.g., Fe or Ni) to assist the guidance of catalytic motors (nanorods, microtubes). The fixed orientation of the micromotors in an applied direct current (DC) magnetic field and thus their direct motion relies on the shape anisotropy of, e.g., tubular [46, 47, 51] or rod-like objects [42, 52, 53]. However, this cannot be applied to objects with high symmetry spherical particles. To achieve a controlled motion of spherical objects, thin films with out-of-plane magnetic anisotropy should be used [41]. Briefly speaking, this approach relies on the specific properties of magnetic films that decorate the spheres but not on their shape. More specifically, ultrathin multilayers of Co/Pt, deposited on top of silica or polystyrene beads, have been used to control the motion efficiently [41].

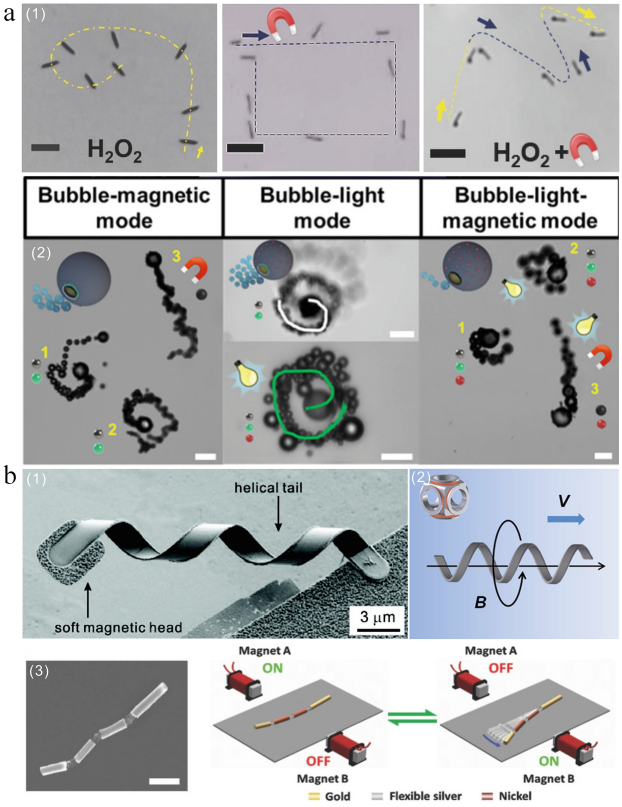

Fig. 7.2 **A** Applying magnetic fields for navigation and actuated by other propulsion sources. (1) Time-lapse image showing magnetic manipulation and propulsion of a hybrid TiO_2-PtPd-Ni NTs along a preplanned trajectory. Adapted with permission from [48]. Copyright ©2016 WILEY-VCH Verlag GmbH and Co. KGaA, Weinheim. (2) Image shows the hybrid propulsion modes of a GDYO/Pt-Fe_2O_3-QDs Janus micromotors in hydrogen peroxide solutions. Adapted with permission from [49]. Copyright 2020 American Chemical Society. **B** External magnetic field that actuates the motion of propelled micro/nanomotors. (1) An artificial bacterial flagellum consists of helical tails fabricated by the self-scrolling of helical nanobelts and soft-magnetic heads. Adapted with permission from [50]. Copyright ©2009 American Chemical Society. (2) Plant-based bioinspired magnetically propelled helical microswimmers. Adapted with permission from [44]. Copyright ©2013 American Chemical Society. (3) The multilinked artificial nanoswimmer consists of a gold head, two nickel bodies, and one gold caudal fin, with three porous silver hinges connecting each segment and powered by a planar oscillating magnetic field. Adapted with permission from [43]. Copyright ©2016 WILEY-VCH Verlag GmbH and Co. KGaA, Weinheim

On the other hand, in the second group of motors (Fig. 7.2B), the locomotion is dependent on the geometry of the micro-objects and the external magnetic field that actuates the motion [43, 44, 50]. For example, the first helical micromotors were demonstrated by Fischer [54] and Nelson [55] and their co-workers more than a decade ago. Plant-based magnetically driven helical micromotors appeared in 2014,

which can convert rotation around its helical axis into a translational corkscrew motion under a rotating magnetic field. Xylem fibers isolated from spiraled vessels of plants have been coated with thin magnetic layers to create micromotors. It is possible to reach high propulsion speed (over 250 μm/s) and control its directionality with a high precision [44]. Because of the possibility of remote control and actuation of the motion, fuel-free operation, such magnetic micro/nanomotors represent a good candidate for multiple life science applications [30, 56], e.g., efficient penetration through the tissues without visible adverse effects. Li et al. introduced a scale-down of such systems—body-deformable biomimetic magnetic nanomotor that successfully emulates the fish propulsion. The multilink artificial nanomotor has a fish-like head segment, two nickel segments, and a gold segment that forms the caudal fin, all of which are connected by three porous silver hinges [43].

7.2 The Role of Asymmetry in the Generation of Motion

7.2.1 Scallop Theorem

"Rules of the game" that should be obeyed to generate the net motion at the micro/nanoscale are distinct from those at the macroscale. First, a small microscopic particle is strongly influenced by thermal fluctuations and reveals the random Brownian motion [57]. Further, particles moving in the fluid environment are governed by inertia and viscous forces (Eq. (7.1)). The ratio of these two forces determines the so-called Reynolds number (Re)—a dimensionless parameter that qualitatively captures the characteristics of the flow regime. As the particle size decreases down to micro or nanoscale, the inertial force becomes negligible compared to viscous forces [58]. Reynolds number can be described as follows:

$$\mathrm{Re} = \frac{\text{inertial force}}{\text{viscous force}} = \frac{\rho u L}{\mu}, \tag{7.1}$$

where ρ is the fluid density, L is the characteristic linear dimension of the object, u is the flow speed, and μ is the dynamic viscosity of the liquid. For a large-scale motor (large L), for example, human in a swimming pool—the Reynolds number is around 10^4, the human changes their body shape to move forward. Due to the inertial force, human swimmer continues to move in water for some time after body shape change stops. In contrast, for the small-scale objects (small L) (e.g., micro/nanoobjects, chemotactic cells, and bacteria), their Re numbers are very small. For example, a swimming bacteria, Escherichia coli (*E. coli*) swims at Reynolds number as low as 10^{-4} moving their flagella by using rotary motors embedded in the cell walls [35]. Due to low Reynolds number, their inertial force is totally irrelevant compared to the viscous force. Thus, the viscous force dominates the motion. If the flagella of the bacteria stops rotation, the bacteria will terminate the motion immediately. The

absence of the inertial effect at low Reynolds number results in the situation that the conventional propulsion mechanism for macroscale objects cannot lead to any actual movement. Thus, the macroscopic and micro/nanoscale motors require different mechanisms for motion. The traditional mechanical components and batteries are not working anymore at these small scales [59].

To shed light on the necessary prerequisites to maintain the motion at the microscale, the nonlinear Navier–Stokes equations (Eq. (7.2)) should be solved, enabling to predict the character of the fluid flow:

$$\rho\left(\frac{\partial}{\partial t}+\mathbf{u}\cdot\nabla\right)\mathbf{u}=-\nabla p+\mu\nabla^2\mathbf{u},\quad \nabla\cdot\mathbf{u}=0. \tag{7.2}$$

The following assumptions should be taken into account: fluid is an incompressible Newtonian fluid, where μ is the dynamic viscosity, p is the pressure, t is time, and $\mathbf{u}$ is the vector of the flow velocity. In the case of low Reynolds number ($\mathrm{Re}\rightarrow 0$), the Navier–Stokes equation can be simplified to the linear and time-independent Stokes equations (Eq. (7.3)):

$$-\nabla p+\mu\nabla^2\mathbf{u}=0,\quad \nabla\cdot\mathbf{u}=0. \tag{7.3}$$

For the objects with Reynolds number $\mathrm{Re}>1$, the net displacement can be achieved with non-reciprocal motion. As shown in Fig. 7.3A, the scallop with $\mathrm{Re}>1$, can move forward by opening its shell slowly and closing its shell fast, squirting out water. Imagining the scallop at a low Reynolds number ($\mathrm{Re}\ll 1$), the same motion strategy will not work anymore, as the time component in the opening/closing of the shell can be neglected. As a result, the scallop cannot reach a net displacement but just generate a series of back and force movements, no matter how fast or slow they open and close their shell. This example lies in the basics of the so-called "*scallop theorem*" [60]. In turn, the type of motion, where body shape changes to a certain configuration, followed by the reversing to its original shape with the exact reversed sequence is called—a *reciprocal motion*. Hence, a micro/nanomotor must generate a non-reciprocal motion to produce a net displacement. Purcell described non-reciprocal motion in his lecture and paper "*Life at low Reynolds Number*", as described in Fig. 7.3B. Thus, to induce movement at low Reynolds number, *time-reversal symmetry* has to be broken.

7.2.2 Asymmetry of the Micro/Nanomotors

Figure 7.4 summarizes five strategies to break the Scallop theorem. (S1) Asymmetry is an important requirement to design movable micro/nanomotors. Asymmetric geometries such as tubular, helix, fish-like, rod-like can be considered for these purposes. (S2) Another solution would be a fabrication of micromotors, mimicking biological motors that have their recipes to move at the microscale, e.g., particles

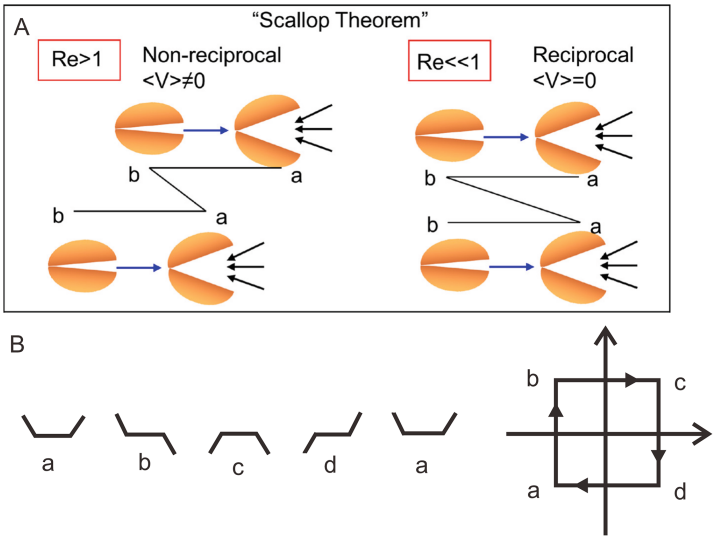

Fig. 7.3 **A** Schematic image of Purcell's scallop presenting a non-reciprocal motion in a high Reynolds number fluid and reciprocal motion in a low Reynolds number fluid with no net replacement (so-called "Scallop Theorem"). Adapted with permission from [31]. Copyright ©2021 American Chemical Society. **B** The two-hinged theoretical swimmer proposed by Purcell: the non-reciprocal series of angle configuration results in a net displacement after a whole cycle. Adapted with permission from [60]. Copyright ©1977, AIP Publishing

with the artificial flagellum. (S3) Then, a non-symmetric magnetic field can also be used to drive symmetric micro-objects. (S4) Actuating a magnetic object close to a boundary (e.g., wall, interface) can also break the spatial symmetry. (S5) Finally, it is important to note that the scallop theorem only works for Newtonian fluids. Time-reversible reciprocal motion can still generate an effective propulsion in non-Newtonian fluids [31].

7.2.3 Symmetry Breaking to Get Deterministic Motion of the Micro-/Nanomotors

The magnetic actuation of mobile micro-/nanomotors relies on time-varying magnetic fields and spatial gradients (Fig. 7.5) [31]. Magnetic actuation can be realized via placing a microscopic object decorated by the magnetic elements (deposited films, magnetic particles, particles flexible magnetic chains, stripes, etc.) in a magnetic field. When a magnetic field is applied, a magnetic body tends to align its easy magnetization axis with the direction of the applied magnetic field (magnetic field actuation of macroscopic objects is described in Chap. 8). If the magnetic field is rotated, then the body rotates by virtue of a generated magnetic torque **T** between the magnetic moment **m** of the body and the applied magnetic field **H**, as follows:

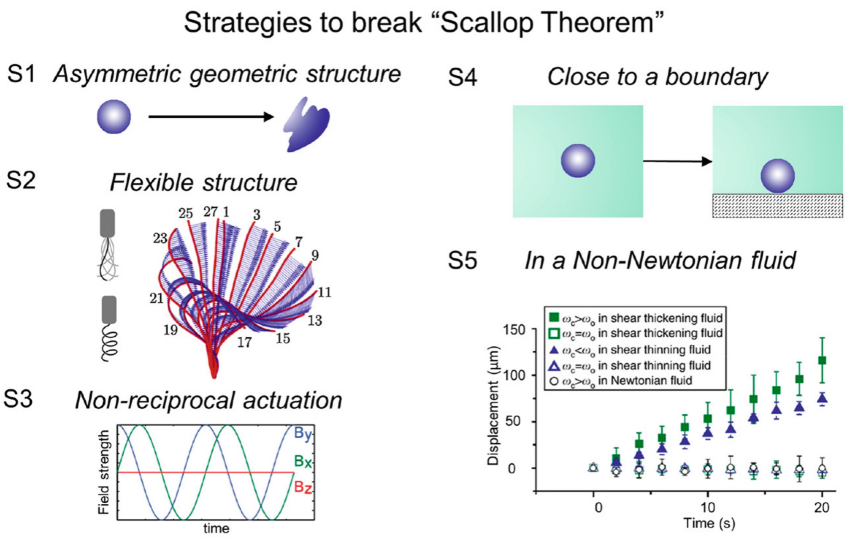

Fig. 7.4 Summary of the strategies to break the "Scallop Theorem" to produce an efficient movement. (S1) Fabricating a small-scale robot with an asymmetric shape. (S2) Creating a micro- or nanostructure containing a flexible component. (S3) Using nonsymmetric actuation with a magnetic field. (S4) Actuating small-scale magnetic devices in the proximity of a boundary (e.g., wall, interface) to break the spatial symmetry. (S5) Propulsion in non-Newtonian fluids. Adapted with permission from [31]. Copyright ©2021 American Chemical Society

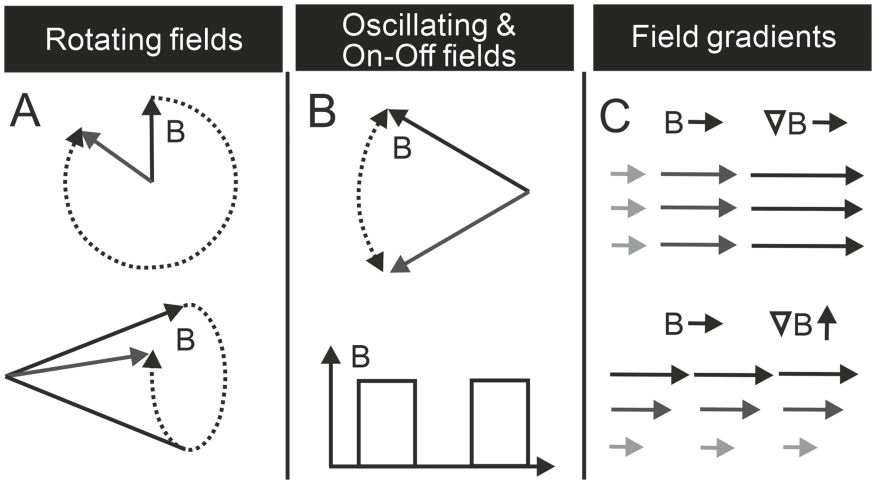

Fig. 7.5 Magnetic actuation modes. **A** Rotating field: Field vector rotated in a plane (top). Field rotated along the mantel of a cone (bottom). **B** Oscillating "up-down" field in a plane (top). On-off field (bottom). **C** Magnetic field gradients. Adapted with permission from [61]. Copyright ©2013 Royal Society of Chemistry

$$\mathbf{T} = \mu_0 \mathbf{m} \times \mathbf{H}, \tag{7.4}$$

where μ_0 is the permeability of free space.

As shown in Fig. 7.5, a continuous drive under a magnetic field requires either a spatial variation, for example, a field gradient, or a temporal variation, such as rotating, precession, oscillating, or in an on-off state [61]. Inspired by the swimming strategies employed by the eukaryotic and prokaryotic microorganism, generating thrust by the sinusoidal-like beating and the corkscrew rotation of flagellum, respectively, helical micro/nanomotors propelled by the rotating magnetic fields have been developed [56, 62]. Magnetoelastic filaments (micro/nanostructures containing flexible components) can also be used to mimic the mobile behavior of sperm by coupling with sinusoidal magnetic fusion. This swimmer initiates wave propagation through the paddle-like beating of its flying tail, moving mainly from its free end to the tethered end [62]. Furthermore, using an asymmetric actuator magnetic field, a small symmetric structure can perform translational motion using a traveling wave or cilia beating mechanism. In addition, there are also realizations where there was shown a possibility to drive a small magnetic device based on surface assistant propulsion, which relies on the proximity to breaking the spatial symmetry [31]. On the other hand, instead of relying on actuating effect of the magnetic forces and torques, the applied AC magnetic field can also be used to induce the thermophoresis—the self-diffusive propulsion of an object in any liquid medium due to a local temperature gradient, formed around the spherical particle [40]. Within this approach, the external field is applied to induce thermophoretic motion of Janus particles via local heating a cap of the particles, e.g., due to the hysteresis losses within the thin films. All these approaches prove that either the asymmetric geometry involving the magnetic thin films or flexible or shapeable building blocks are necessary to initiate the net motility of the micro/nanomotors.

In the following, we review different examples of magnetic micro/nanomotors in detail. Curvilinear magnetic films are used either to generate the net propulsion via actuation of its shape or to rectify the Brownian motion via suppression of the rotational component of the diffusion.

7.2.3.1 Spherical Micro/Nanomotors and Their Assemblies

In all following experimental demonstrations, micromotors were dispersed in an aqueous solution and dropped onto the glass slide to observe their behavior. Videomicroscopy is used to record the motion of the particles. AC or DC magnetic field is applied via a nearby placed set of Helmholtz coils.

The idea to use the spherical micromotors was first demonstrated in 2007 [63] and attracted strong attention from the interdisciplinary community of physicists, chemists, material scientists, micro-robotics, and biomedical researchers. Such motors, so-called Janus particles, are represented by microscopic (1–10 μm) colloidal particles, i.e., fused silica or polystyrene (PS), which are half covered by thin metal layers. These films are the catalysts (e.g., platinum for H_2O_2 decomposition)

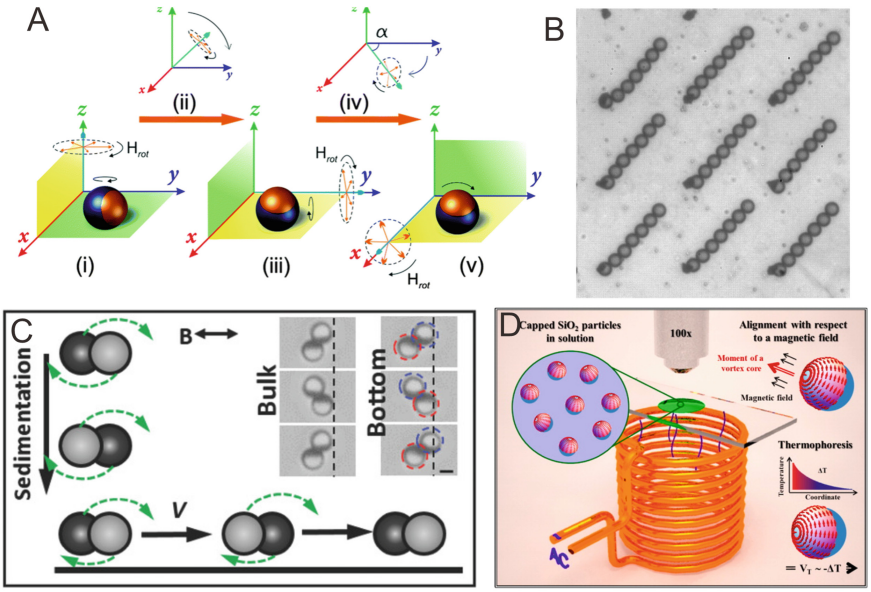

Fig. 7.6 **A–C** Magnetic surface walkers. **A** Schematic illustration of manipulating single Janus microsphere by an in-plane rotating magnetic field on a surface. Adapted with permission from [64]. Copyright ©2016 Royal Society of Chemistry. **B** Assembly of artificial cilia. Artificial biomimetic cilia are composed of chains of spherical superparamagnetic particles that self-assemble in an external magnetic field. Magnets can also be used to actuate the cilia in a simple non-reciprocal manner, which results in fluid flow. Adapted with permission from [71]. Copyright ©2010 National Academy of Sciences. **C** Janus microdimer surface walkers propelled by oscillating magnetic fields. A magnetic Janus microsphere forms a microdimer via magnetic dipolar interactions, and this microdimer rolls its two "feet" back and forth in an alternate manner. These surface walkers can navigate through complicated structures using an oscillating magnetic field. Adapted with permission from [68]. Copyright ©2018 WILEY-VCH Verlag GmbH and Co. KGaA, Weinheim. **D** Magnetically induced thermophoretic motion. The particles are propelled by a thermophoretic force resulting from a temperature difference at both ends of the capped particle exposed to the AC magnetic field. Adapted with permission from [40]. Copyright ©2012 American Chemical Society

or can be converted to a catalyst (e.g., Ag conversion to AgCl for photocatalytic decomposition) for the local chemical reactions near the surface of the Janus particle, leading to the motion of the particle. In the presence of an external magnetic field, reorienting the entire magnetic Janus particle achieved through the addition of a magnetic film helps to realized the deterministic motion behavior of such objects over a longer period (further details on the fundamentals of magnetically capped spherical particles can be found in Chap. 3). Their driving mechanisms can be divided into three different categories, including: (i) "surface walkers" approach (Fig. 7.6A–C), (ii) magnetically induced thermophoresis (Fig. 7.6D), and (iii) motion guidance using an external magnetic field.

(i) *Magnetic surface walkers* are micro/nanomotors that move on a surface under a rotating or oscillating magnetic field. As a result of the friction between the

micro/nanomotors and the surface, forward motion is generated [56]. This type of motor relies on a surface to break the spatial symmetry and provide an additional degree of freedom to escape the scallop theorem [35]. Figure 7.6A schematically illustrates the manipulation of a single Janus microsphere by an in-plane rotating magnetic field. The magnetic Janus micromotors [64], uniform microspheres [65], clusters [66], and colloidal chains [67], are able to perform the rolling motion at the surface under magnetic field (Fig. 7.6B). For example, Li et al. [68] reported the propulsion and steering of magnetic micro dimmers in an oscillating magnetic field: two Ni-dielectric Janus spheres in the dimer rolled alternatively, step by step. Another prominent example demonstrates the use of superparamagnetic colloids and rotational magnetic fields to create reversible close-packed assemblies (microwheels) that subsequently spin due to their net dipole interacting with the dynamic applied field [66]. When particles move far away from the substrate, the friction between the micro/nanorobots and the substrate surface disappears. Then particles which are rotated with a magnetic field will not acquire any net displacement [68].

(ii) It is known that the motion of spherical Janus micromotors can be generated by forming e.g., chemical or thermal gradients around the particle cap (e.g., catalytic motors). Obviously, there should be a possibility to use an external magnetic field, acting on magnetic thin films within the cap, to generate such a gradient. This idea has been realized as follows: an AC magnetic field (in kHz range) is applied to induce a thermophoretic motion of the objects due to heating of a magnetic cap of the particles; at the same time, an additional DC magnetic field is used to orient Janus motors and guide their motion (Fig. 7.6D) [31]. Control of the motion is achieved due to specific properties of 100-nm-thick Permalloy (Py, $Fe_{19}Ni_{81}$ alloy) magnetic films offering a topologically stable magnetic vortex state within the cap of Janus motors (Fig. 7.7A). Thus, *magnetically induced thermophoretic* locomotion in this realization does not require catalytic chemical reactions that imply toxic reagents.

(iii) Spherical micro/nanomotors can also use external magnetic forces to control the direction and speed of the micromotor. At the same time, the motion itself is generated by other means [40, 41]. While spherical micromotors driven by chemical reactions, photo-induced photochemistry, or even acoustic motors do not have directional control on default, the additional magnetic layer (e.g., nickel [12, 22], cobalt [69], and iron oxide [70]) has been widely adopted and can be embedded in micromotors to adjust and reorient their motion and improve the controllability of these motors' movements [3, 31]. The magnetic materials with in-plane magnetic easy axis, such as iron or nickel films, cannot be applied to spherical Janus particles due to the high symmetry of the particles. In this respect, Baraban et al. used specific properties of ultrathin Permalloy magnetic films (Fig. 7.7A), with a topologically stable magnetic vortex state in the cap structure of Janus motors [40]. A vortex has a specific magnetization distribution, and it is thus magnetically compensated everywhere except the core. This uncompensated component of the vortex can manipulate the moving direction of the Janus micromotor. Furthermore, Baraban et al. applied a different strategy to realize the directed motion of Janus swimmers by preparing ultrathin $[Co/Pt(Pd)]_N$ magnetic multilayer cap structures on spherical non-magnetic particles (Fig. 7.7B) [41]. This particular magnetic film possesses a

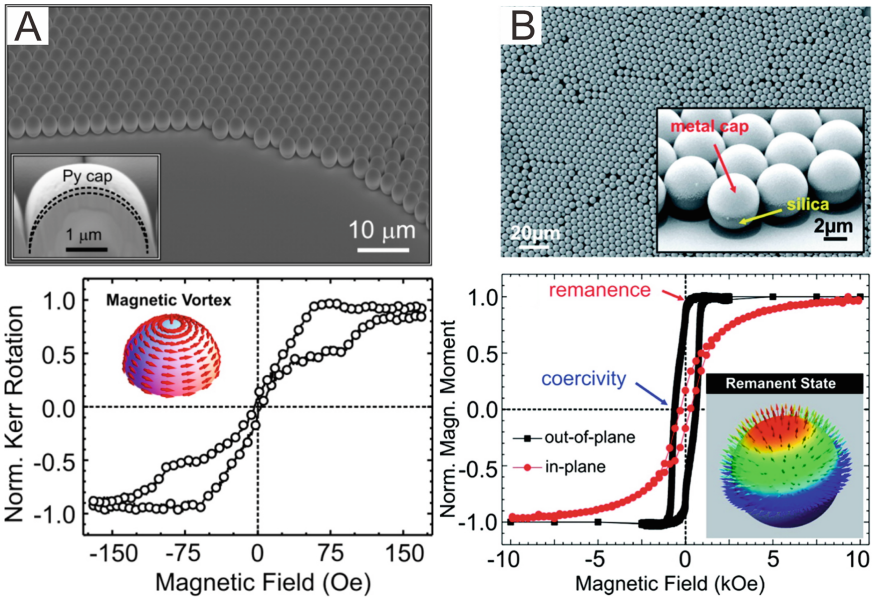

Fig. 7.7 **A** Janus micromotor for magnetically induced thermophoresis and their magnetic hysteresis loop. A DC magnetic field is used to orient Janus motors and guide their motion on a long time scale, while an AC magnetic field is applied to induce thermophoretic motion of the particles by heating a magnetic cap. Adapted with permission from [40]. Copyright ©2012 American Chemical Society. **B** Janus motors with multiple magnetic layers $[Co/Pt]_5$ exhibit a well-defined magnetic axis easy that coincides with the symmetry axis of the cap. Due to the magnetic configuration of the system, the Janus particle can be controlled perfectly, and direct manipulation of the cargo can be accomplished directly by varying the magnetic field spatially. Adapted with permission from [41]. Copyright ©2012 American Chemical Society

well-defined perpendicular magnetic anisotropy and high remanence (80–90 % of the saturation magnetization). In this case, when used in remanence after magnetic saturation, the magnetic cap of the micromotor can be aligned with the external magnetic field by physical rotation of the sphere at a small external magnetic field (< 10 Oe). In addition, the motion can be stopped by spatially changing the direction of the magnetic field as needed [41].

7.2.3.2 Rod-Like Micromotors

In contrast to spherical objects, rod-like particles possess built-in asymmetry: object has long and short symmetry axes. When the rod-shaped micromotors are placed in an external magnetic field, they can be driven by a rotating magnetic field with tumbling motion, which relays on the boundary to break the symmetry and achieve propulsion (Fig. 7.3) [45, 52, 72]. Zhang et al. reported nickel nanowires swimming near a patterned solid surface and demonstrate colloidal cargo transport. The nanowires can

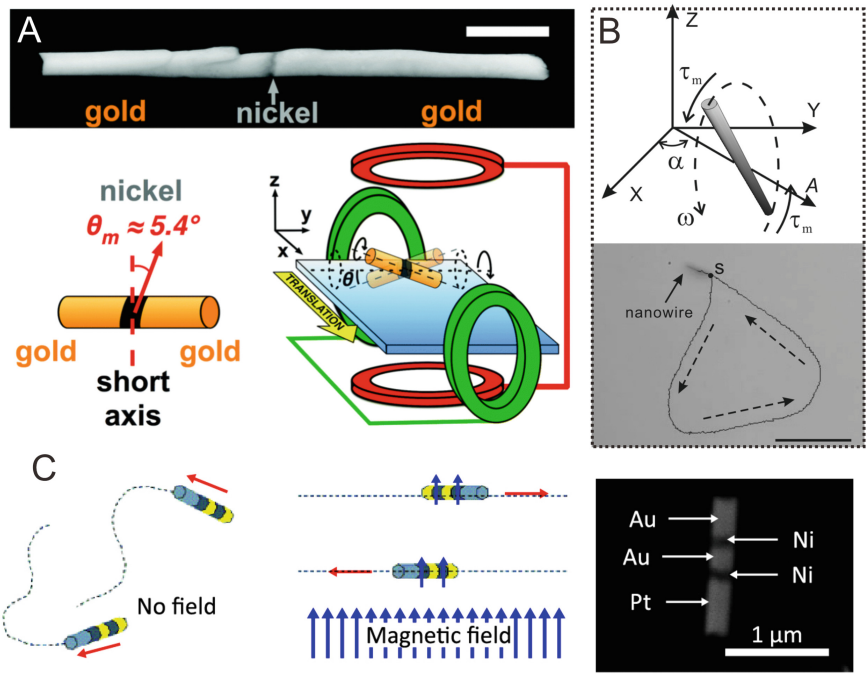

Fig. 7.8 Rod-shaped micromotor driven by the rotating magnetic field near a surface. A gold-nickel-gold microrods precessing at 1 kHz rotation magnetic field near a solid–liquid interface. Adapted with permission from [45]. Copyright ©2017 Royal Society of Chemistry. **B** Nickel nanowire rotating vertically with respect to the XY-plane and travels along the tracking line near a flat surface. Adapted with permission from [53]. Copyright ©2010 American Chemical Society. **C** Controlling the direction of striped nanorods in an applied field. Adapted with permission from [42]. Copyright ©2005 WILEY-VCH Verlag GmbH and Co. KGaA, Weinheim

be propelled and steered by a tumbling motion, i.e., rotation plus translation (ACS nano 4.10 (2010):6228–6234). Mair et al. demonstrate gold–nickel–gold microrods precessing at 1 kHz rotating magnetic field near a solid–liquid interface, achieving speeds of 14 μm/s [45]. Figure 7.8A, B summarizes the aforementioned statements and the examples from the literature.

As mentioned in the previous section for spherical micromotors, magnetic fields are not only used to induce the motion via actuation but also are useful for controlling the direction of rod-like micromotors. By using an external magnetic field, Kline et al. presented a method for manipulating the directions of so-called "striped" nanorods, which consist of several segments—stripes. These different segments play an important role in the striped rods (Fig. 7.8C). The platinum segment acts as a catalyst for the decomposition of hydrogen peroxide, which together with the gold film leads to the self-electrophoresis of the whole object. The ferromagnetic nickel segment can be magnetized and used to control the direction of rod movement. Please note that in contrast to the micromotors with the spherical symmetry, *in-plane* magnetic

anisotropy of the ferromagnetic films, e.g., Ni, is sufficient to control the orientation of the *rod-like structures*. Electroplating methods are used to deposit thin nickel films (Fig. 7.8A). In such configurations, the rod is *magnetized transversely* rather than longitudinally [42]. In the presence of a magnetic field, most rods turn perpendicular to the magnetic field lines and move towards the platinum end.

7.2.3.3 Tubular Systems

The tubular micromotors hold great promise to be used as an efficient tool for manipulation of the microbes and cells (further details of the fundamentals of the magnetic nanotubes can be found in Chap. 4). The tubular microbots are traditionally fabricated using so-called "rolled-up" technology—using highly strained metal and dielectric nanomembranes, which compacts planar films into three-dimensional tubular architectures (Fig. 7.9A) [73–75]. Alternatively, the template electrodeposition (see also Chaps. 2 and 5) [76, 77] and template-assisted layer-by-layer assembly [78] can be used for high throughput fabrication of microbots. Tubular micro/nanomotors offer several advantages, e.g., easy motion control, integration of various functions, scalable size in diameter and length, and straight trajectories [47]. By incorporating a

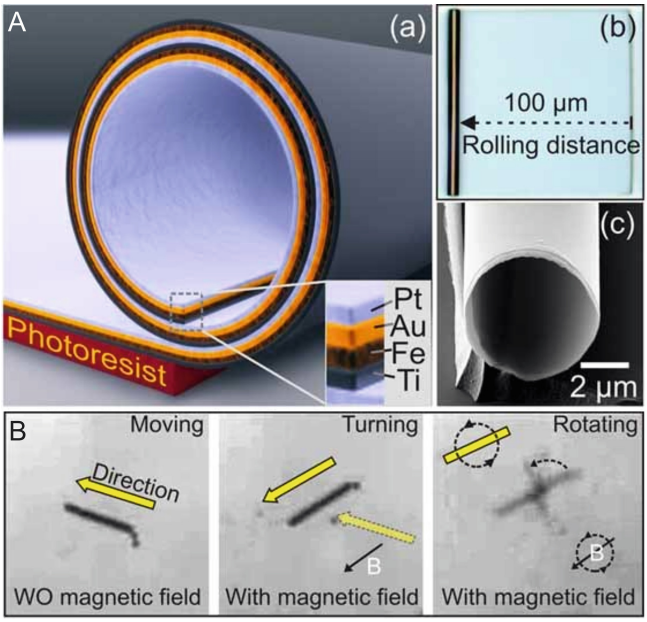

Fig. 7.9 **A** Schematic diagram of a rolled-up microtube consisting of Pt/Au/Fe/Ti multilayers on a photoresist sacrificial layer. **B** Remote control of a catalytic microjet by applying an external magnetic field, thus turning and rotating the microtube. Adapted with permission from [73]. Copyright ©2009 Wiley-VCH Verlag GmbH and Co. KGaA, Weinheim

magnetic component into the microtube, the direction of the micromotors can be controlled by an external magnetic field. Solovev et al. [73] demonstrated a catalytic microtube self-propelled by gas bubbles. They engineer a rolled-up microtube with an inner catalytic surface, serving both as the chemical reaction chamber as well as the gas-collecting cavity. The tube shape asymmetry along the axis determines the moving direction. A sandwiched Fe layer is integrated into the tube wall, enabling to remotely control the motility direction of the catalytic microtube (Fig. 7.9B).

7.2.3.4 Helical Systems

Helical architectures have been widely employed in small-scale robotic systems (further details on fundamentals of magnetic helices can be found in Chap. 2; Chaps. 5 and 6 offer further remarks on the fabrication and characterization of these objects, respectively) [28, 79]. These structures can be actuated in fluids and display *translational corkscrew motion* when they are subject to low-frequency rotating magnetic fields. As mentioned in Eq. (7.4) above (Sect. 7.2.3), magnetic torque **T** is directly proportional to the applied magnetic field **H**. To achieve corkscrew motion, the magnetic field should rotate in a plane orthogonal to the long axis of the helix. The propulsion force **F** and **T** are linearly related to the velocity u and the angular speed ω by the following propulsion matrix:

$$\begin{bmatrix} F \\ T \end{bmatrix} = \begin{bmatrix} a & b \\ c & d \end{bmatrix} \begin{bmatrix} u \\ \omega \end{bmatrix} \tag{7.5}$$

where a, b, c, and d are constants that are proportional to the viscosity of the fluid and depend on the shape and size of the swimmer [60, 61]. The helical swimmer's velocity in general increases linearly with increasing the rotational frequency of the magnetic field up to the maximum frequency, known as the step-out frequency. Below the step-out frequency, magnetic helices swim synchronously with the magnetic field. Above the step-out frequency, the magnetic moment of the helix rotates asynchronously with the rotating magnetic field, and the velocity of the swimmer decreases upon increasing the frequency.

A suitable selection of materials and particular designs are crucial in magnetic helical propellers [80]. Figure 7.10 shows different types of magnetic helical robotic designs. Type I corresponds to a small-scale robot with a magnetic head and a non-magnetic helical tail. In this case, the magnetic head should display a preferential magnetization axis, in other words, magnetic anisotropy (shape or crystalline), to be able to rotate under a rotating magnetic field. A ferromagnetic structure, like the rectangular head in type I helical small-scale robot would exhibit an easy magnetization axis across the basal plane (Fig. 7.11A, Type I). A rotating magnetic field would cause the rotation of the head together with the attached helical tail leading to a corkscrew-type propulsion. Régnier and co-workers realized an investigation that concluded that the shape of the head of a helical swimmer does not affect the propulsion curve but it does influence the step-out frequency [80]. The second type

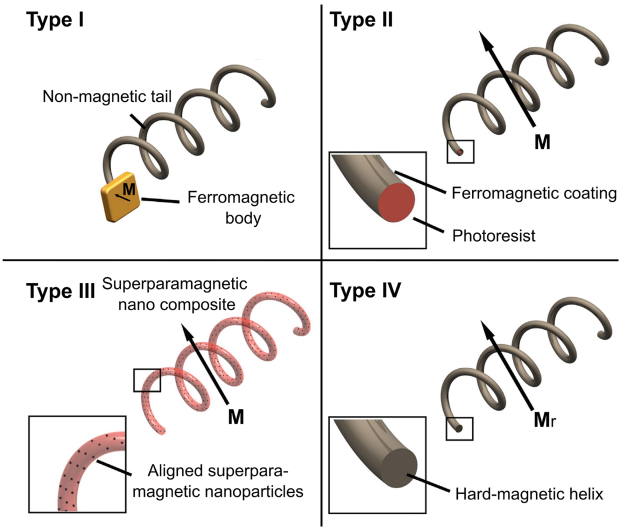

Fig. 7.10 Types of magnetic helical robotic designs. A magnetic head with a non-magnetic tail constitutes a type I robot. Type II is a non-magnetic helical skeleton coated with a thin ferromagnetic layer. Type III depicts a helical composite formed by a polymeric matrix embedded with magnetic nanoparticles. Type IV is a fully ferromagnetic helix. Adapted with permission from [81]. Copyright ©2018 WILEY-VCH Verlag GmbH and Co. KGaA, Weinheim

in Fig. 7.10 corresponds to a non-magnetic helical chassis conformally coated with a magnetic layer. The chassis could be made of a photoresist, a ceramic, or a metal. In such designs, the swimmers display two directions of magnetization [81] (Fig. 7.11A, Type II), being M_1 and M_2 the magnetizations perpendicular to and along the helical axis, respectively. M_1 contributes to the propulsion of the swimmer, while M_2 causes its wobbling. The third type embraces small-scale composite helices consisting of a polymeric matrix containing dispersed magnetic nanoparticles [82]. Rubinstein and co-workers developed a numerical approach to study this type of helices that revealed that the magnetic anisotropy and polarizability of this type of helices are determined by the filament cross-section elongation and orientation [82]. The authors concluded that slender helices display an easy axis along the helical axis and are poor propellers. In contrast, tight helices exhibit a preferential magnetization in a transverse plane with respect to the helical axis and are more efficient propellers. Figure 7.11B, C shows the orientation of the easy magnetization axis Φ with respect to the helical axis as a function of the pitch angle Θ of four different types of helices. It can be seen that for low Θ, all helices have an easy magnetization axis along the helical axis. Increasing the pitch shows that regular, normal, and magnetic polymer composite (MPC) helices transition to a traverse easy magnetization axis (further details on the actuation of magnetic composites as magnetic soft robots can be found in Chaps. 8 and 9). MPC refers to the type of helices reported in [82], in which the filament cross-section is elongated in a fixed direction in a plane approximately transverse to the long axis

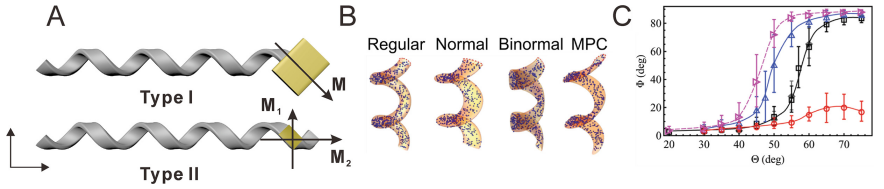

Fig. 7.11 **A** Experimental images of type I and type II helical motors of 10 cm in size. Type I has on its head NdFeB permanent magnets of millimeter size with the preferential magnetization axis (**M**) parallel to the basal plane. NdFeB permanent magnets coat only the first-full-turn portion of the helix in the type II robot. Two directions of magnetization (M_1 and M_2) contribute to the dynamic properties of the type II microrobot. Redraw based on [80]. **B** Illustration of helical composites of type III, consisting of a polymeric matrix embedded with magnetic nanoparticles. Regular, normal, and binomial helixes have a ring-shaped top view horizontal projection. The orientation of the elliptical filament cross-section is varied in each helix by changing the aspect ratio. The cross-section is increased and reduced by three-fold in normal helixes and binormal helixes, respectively. For the regular helix, the aspect ratio is kept constant along the helix axis. The last illustration is the magnetic polymer composite (MPC). It presents a fixed elongation in the direction transverse to the helical axis that distorts the ring-shaped horizontal projection into an elliptic shape. **C** The graph shows a theoretical simulation of effective magnetizing. Φ is the inclination angle of the easy axis. The graph shows Φ as a function of the helix angle Θ for regular (□), normal (△), binormal (◯), and MPC helixes (▷). Panels B, C are adapted with permission from [82]. Copyright ©2016 Royal Society of Chemistry

of the helix. Alignment of particles can also be used to adjust the orientation of the preferential magnetization axis (programmed anisotropy [83]) for any type of helix design as reported in [84], thus minimizing the influence of shape in the magnetic polarizability of the helix. Figure 7.12A shows single twist composite microhelices, one with randomly distributed particles (labeled as "reference" in the figure), and another with particles aligned perpendicularly to the helical axis (labeled as "manipulated" in the figure). Upon application of rotating magnetic fields, the reference helix tumbles, while the manipulated one is able to swim in a corkscrew fashion. To change the direction of the swimmers, the plane of the rotating magnetic field is changed. The last type of helix consists of a fully metallic ferromagnetic chassis. In this case, to display a corkscrew motion is usually more convenient to construct the helix out of a hard-magnetic metal or alloy, as these materials can generally retain a large magnetization after being magnetized [80]. As such, pre-magnetizing the helix in a direction perpendicular to the helical axis enables the helix to perform corkscrew motion more efficiently. Figure 7.12B, C shows 3D printed biodegradable magnetic small-scale helices made of sucrose containing hard-magnetic microparticles of barium ferrite [85]. Prior to their manipulation, the helices are magnetized perpendicularly to the helical axis.

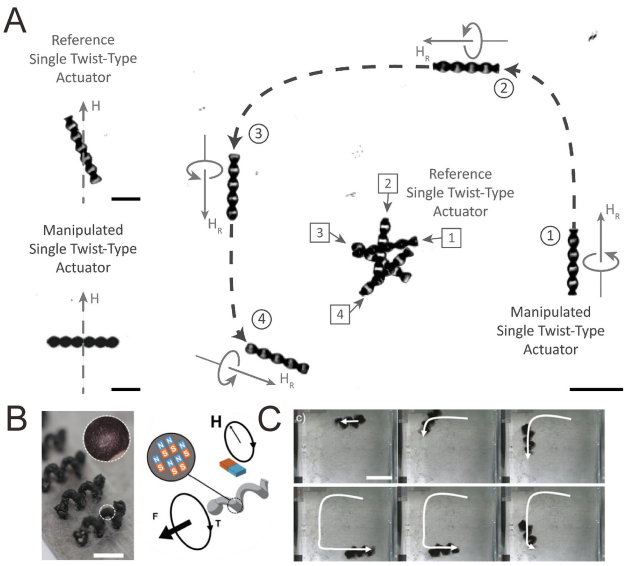

Fig. 7.12 **A** Single-twist helical microrobots with programmed magnetic anisotropy. These micromotors were produced by two-photon polymerization (further details on the technique of two-photon polymerization can be found in Chap. 5) of superparamagnetic magnetite nanoparticles dispersed in a photocurable resin (SU8). In reference single twist-type actuator, single domains magnetic nanoparticles are distributed randomly, and the geometric effects determine the magnetic properties of the robot. The application of a magnetic field during the curing process magnetizes the single domain particles, which turns their magnetic moment parallel to the external field. This process decouples the final magnetic properties of the robot from geometric effects and allows to tune the magnetic properties of the robot. The first image shows the outcome of applying a magnetic field with a device pitch angle of 45° over the reference and manipulate single-twist helical microrobots. The magnetic easy axis given by the shape anisotropy is parallel to the rotational axis in the reference robot. Here, the robot slightly tilts its magnetic easy axis away from the external field. The manipulated robot orients perpendicular to the applied magnetic field due to the pre-realignment of the domains. The scale bar is 20 μm. The second image shows the dynamic properties of the micromotor when a rotating magnetic field is applied over the reference and manipulated robot. Manipulated single-twist helical robots perform a corkscrew-propulsion, whereas the reference single-twist helical robot rotates about its center of gravity. The scale bar is 50 μm.Adapted with permission from [84]. Copyright ©2014 WILEY-VCH Verlag GmbH and Co. KGaA, Weinheim. **B** Helical sucrose composite embedded with programmed magnetic barium ferrite nanoparticles. The first image is a bright field photograph of the robot after 3D printing via selective laser sintering (SLS). The insert is a higher magnification image of the surface. The second image shows a schematic representation of the robot. A pre-magnetization of the nanoparticles in a transversal direction to the screw axis sets the preferential direction of magnetization. **C** The sequential images depict a corkscrew motion when the robot is dispersed in a liquid under the application of a rotating magnetic field. The scale bar is 10 mm. Adapted with permission from [85]. Copyright ©2020 Wiley-VCH GmbH

7.2.3.5 Shape-Morphing Systems

Shape-morphing small-scale robotic systems refer to those designs that contain one or more component that experiences a physical or a chemical change that ultimately leads to a change in the morphology or shape of the entire robotic ensemble [16]. The capability of shape transformation allows for the robotic systems to adapt to the environment, an ability that is common in microorganisms and cells [86]. Additionally, this property can be advantageous for small-scale motile devices as their locomotion mechanism can also be modulated. As such, shape-morphing micro/nanorobots are being intensively investigated for their potential use in biomedical applications [87, 88]. Shape-morphing systems are usually made of soft flexible materials such as polymers, gels, and peptides, which exhibit more flexibility than other metals such as ceramics or metals, and, subsequently, can morph into complex shapes. Yet, according to Duan and co-workers [89], shape-morphing can also be a property of rigid devices, if some of the components exhibit relative translational or rotational motions upon an applied stimulus. One of the advantages of soft materials in contrast to rigid parts is that they enable the realization of small-scale robots with physicochemical properties closer to those of biological tissues and cells.

In this section, we briefly review magnetic shape-morphing soft robotic systems. A magnetic system that changes its shape or morphology might also change its magnetic anisotropy. This important feature must be considered when designing shape-morphing devices, especially those in which their preferential axis of magnetization determines their locomotion mechanism. This is well illustrated in the contribution by Nelson and co-workers on soft micromotors with programmed motility and morphology [90]. These micromotors are composed of magnetic nanocomposite hydrogel bilayers micropatterned by 2D photolithography (Fig. 7.13A). The bilayer hydrogel consists of a thermally responsive layer with a high degree of swelling and a non-swelling layer. By magnetically aligning particles in each layer during fabrication, it is possible to have components with programmed anisotropy. A prototypical device consists of a bilayered rectangular plate and a non-swelling tail. In the nonresponsive layer (labeled as "supporting layer" in Fig. 7.13B, particles are oriented parallel to the long edge of the plate, while in the swelling layer particles are oriented perpendicularly. In the tail, particles are transversely oriented. As a result, three magnetization axes can be defined. When the 2D structure is immersed in an aqueous solution, the swelling component intakes water causing the structure to self-fold and morph into a microrobotic architecture with a tubular body and a helical tail (Fig. 7.13B). Different designs can be obtained depending on the particle orientation and shape and composition of the 2D layers. The particle alignment in the supported layer and the tail position drive different folding configurations that are ruled by the edge effect and the resultant internal stress distribution. Aligned particles in the non-swelling layer inhibit geometric restrictions and force the folding to be only dependent on the particle organization, allowing to control the folding angle in the head and, thus the corkscrew motion. Figure 7.14A–C shows how the particle orientation in the non-swelling layer determines the folding axis of the structures. Not only the folding axis but also the magnetic anisotropy can be engineered when align-

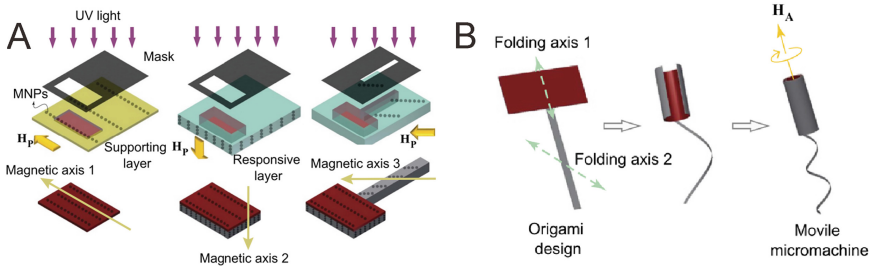

Fig. 7.13 **A** Schematic representation of the 2D photolithography process for the fabrication of micromotors made of magnetic nanocomposite hydrogel bilayers. Flagellated robots are fabricated by sequential micropatterning of the composite. A mixture of photocurable and non-swelling hydrogel mixed with magnetic nanoparticles (MNPs) is introduced in a microchamber to form the supporting layer. A uniform magnetic field ($\mathbf{H}_P$) aligns the particles along the basal plane of the microchamber to induce the first magnetic easy axis 1. Then, the magnetic easy axis 2 is produced by orienting the magnetic field towards the orthogonal direction of the magnetic easy axis 1 and patterning a mixture of the swelling thermo-responsive hydrogel layer embedded in MNPs. The final step implies the magnetic tail formation with its magnetic axis oriented towards direction 3. This tail is formed and attached to the head following the same procedure for the swelling layer. **B** Illustrative representation of the folding process of the flagellated micromotor after dispersion in water. The folding direction is determined by the folding axes 1 and 2. Under a homogeneous rotating magnetic field ($\mathbf{H}_A$), the swimming properties of the micromotor are controlled in a 3D space due to the multiple magnetic axes. Adapted with permission from [90]. Copyright ©2016, The Author(s)

ing particles in the responsive layer. In Fig. 7.14C tubular structures with different preferential magnetic easy axis are obtained. Note that as the swelling layer is thermally responsive, the tubular structure can refold into another tubular configuration by heating, with the responsive layer being initially external and the non-swelling layer becoming external at higher temperature. When the particles in the responsive layer are oriented perpendicular to the largest side of the rectangular plate, the magnetic easy axis is always kept perpendicular to the long axis of the tube both at low and high temperatures. On the contrary, when the particles are aligned parallel to the larger side of the rectangular plate the magnetic easy axis is perpendicular to the long axis of the tube at low temperature, but becomes parallel at higher temperature.

Considering all these features, micro/nanorobots with a rich buffet of motion behaviors and capabilities can be designed.

Hu and co-workers developed a soft-bodied robot that upon the application of magnetic fields can undergo time-varying shape transformations [91]. The robot consists of a sheet of silicone elastomer with embedded hard-magnetic microparticles, and it is magnetized when the sheet is wrapped around a cylindrical rod (Fig. 7.15A). The magnetization profile of the unwrapped robot is shown in Fig. 7.15B. By applying a magnetic field in the XY plane (H_{xy}), it is possible to deform the robotic structure, the shape of which depends on the field's magnitude. Low-magnitude fields curve the robot leading to a sine or cosine shape, while higher fields cause U- or V-shape deflections to the robot (Fig. 7.15C). The richness of locomotion modes of this

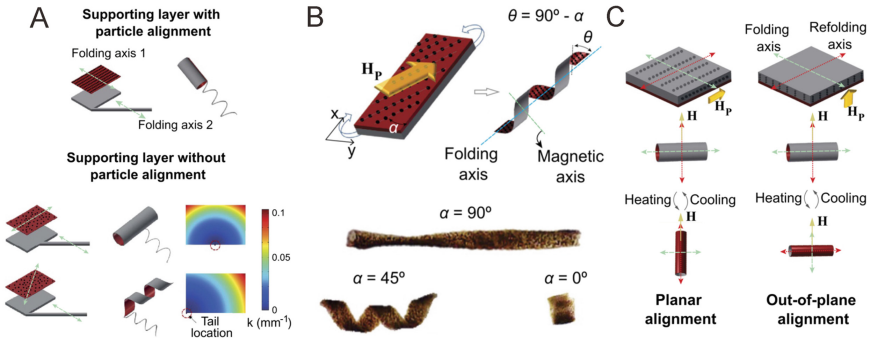

Fig. 7.14 **A** The particle alignment decouples the geometric edge effect of the folding direction in the supporting (non-swelling) layer of the micromotor. Randomly dispersed particles in the first image do not change the geometric folding axis, and the geometric effects govern the bending direction of the layer. Moreover, the tail to the center position in the flagellated micromotor introduces changes in the folding direction of the micromotor head, allowing to have different microrobots with different dynamic properties. Here, finite element modeling shows the internal stress distribution as a function of the tail location. **B** Effect of the magnetic nanoparticle's alignment in the hydrogel bilayer helical structure. Here, α denotes the orientation of the magnetic nanoparticles that generates a helical angle ($\theta = 90° - \alpha$) for the bilayered micromotor. Three examples of α from 90° to 0° are shown. **C** Effect of the particle alignment in the swelling hydrogel layer and shape transformation induced by heat. Out-of-plane alignment allows keeping the bending configuration while the magnetic anisotropy is orthogonal to the folding axis. In the planar alignment configuration, the magnetic anisotropy is parallel to the refolding axis. These refolded configurations change the dynamics of the micromotor from a tumble motion to a corkscrew motion. $\mathbf{H}_P$ denotes the direction of the applied magnetic field during the fabrication process. **H** is a uniform magnetic field used to measure the magnetic anisotropy of the micromotor. Adapted with permission from [90]. Copyright ©2016, The Author(s)

type of robot and the corresponding locomotion modes (i.e., swimming, meniscus-climbing, landing, immersion, rolling, walking crawling, and jumping) are shown in Fig. 7.15D.

Recently, Alapan et al. have shown a strategy for re-programming and high-throughput programming soft robotic components by means of heating magnetic soft elastomeric composites above the Curie temperature ($T = 118\,°C$) of the embedded ferromagnetic chromium dioxide particles and applying magnetic fields during the cooling step [93]. Cui et al. have proposed a strategy based on nanomagnetic encoding to create origami-based shape-morphing microrobots [92]. The robots consist of 2D rectangular magnetic micropanels linked by means of zig-zag hinge springs. Figure 7.16A shows a prototypical micromotor composed of four magnetic panels, two with nanomagnets type I and the other two with nanomagnets type II, all linked to the central nonmagnetic unit. The nanomagnets can be patterned in different sizes, which allow for tailoring their magnetic response (see the magneto-optical Kerr effect hysteresis loops in Fig. 7.16B. In order to encode their response to external magnetic fields, the panels are programmed by applying a sequence of magnetizing fields that will determine their preferential magnetization during the magnetic manipu-

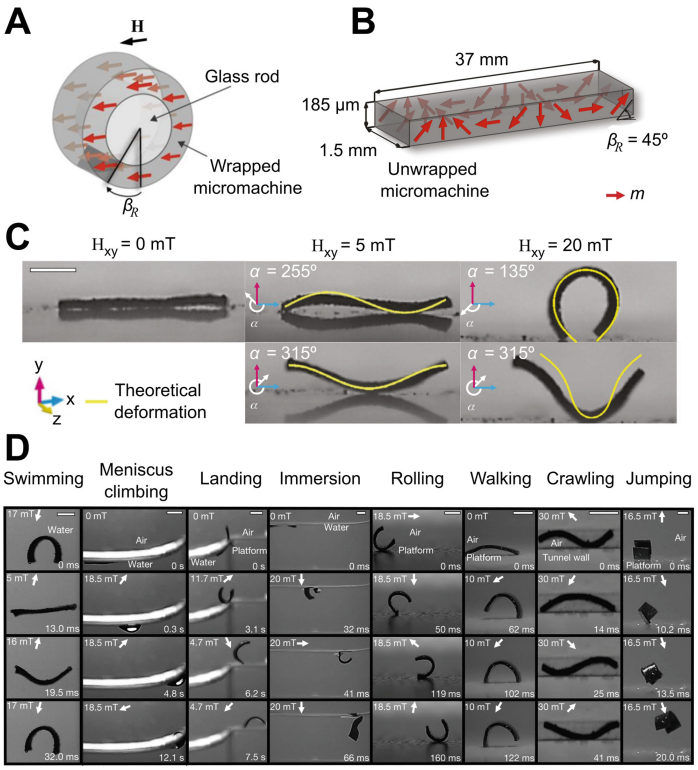

Fig. 7.15 **A** Illustration of a silicone elastomer sheet embedded with hard-magnetic microparticles. The sheet is wrapped around a cylindrical rod under the application of a uniform magnetic field (**H**). This is applied with a vibrating sample magnetometer. The phase shift in the resulting magnetization is determined by the relative orientation. **B** Sketch of the magnetization profile (**M**) in the unwrapped micromotor with phase shift $\beta_R = 45°$. **C** Theoretical and experimental deformations of the micromotor induced by the magnetic field applied in the XY-plane ($\mathbf{H}_{xy}$). α is the angle that describes the direction of $\mathbf{H}_{xy}$ from the x-axis. A small magnetic field induces a sine or a cosine deformation in the micromotor that depends on the direction of the magnetic field. The increase in the amplitude produces a higher degree of curvature, which makes bending the micromotor in a 'C'-shape or a 'V'-shape. Here, the type of deformation depends on the direction of the field applied in the micromotor. The deviation from the model is correlated to a pre-stress introduced by the demolding process. Scale bars, 1 mm. **D** Sequences of dynamic processes that can be induced on the micromotor. Depending on how the magnetic field parameters are applied on the micromotor, swimming, meniscus climbing, landing, immersion, rolling, walking, crawling, and jumping dynamic processes can be achieved by the robot. Scale bars, 1 mm. Adapted with permission from [91]. Copyright ©2018, Macmillan Publishers Limited, part of Springer Nature. All rights reserved

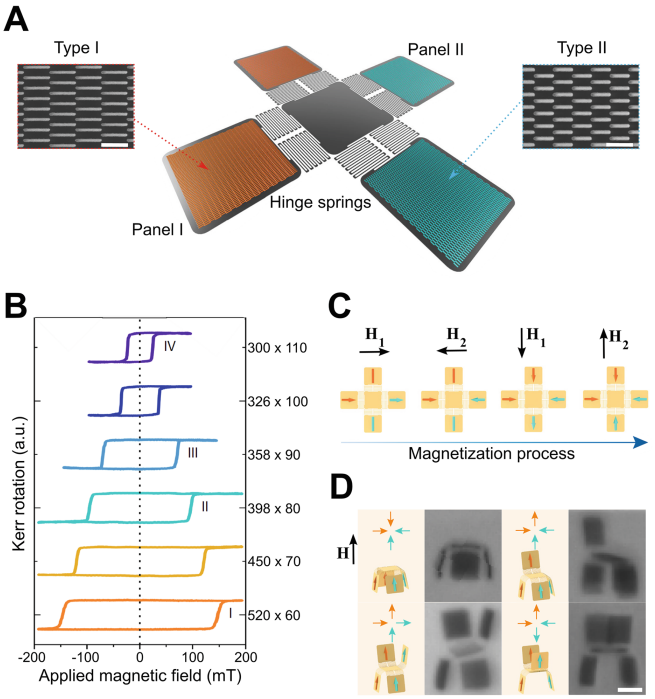

Fig. 7.16 **A** Schematic representation of the four-panel microrobot with type I and type II nanomagnets linked by a zig-zag hinge spring of six turns. The inserts are scanning electron microscopy images of the nanomagnetic arrays for each type of panel. Scale bar, 500 nm. **B** Hysteresis of the magneto-optical Kerr effect measurements for six different aspect ratios (lateral dimensions at the right vertical axis of the graphic) keeping constant the volume. **C** Schematic magnetization process to encode the micromotor folding. Magnetic fields must be sufficient to switch each type of nanomagnets independently. **D** Schematic and experimental bright-field images of the micromotor folding as a function of the panel's configurations. Scale bar, 10 μm. Adapted with permission from [92]. Copyright ©2019, The Author(s), under exclusive licence to Springer Nature Limited

lation. The magnetization process for this prototypical micromotor is displayed in Fig. 7.16C. Different encodings lead to different shape transformations when the micromotor is subject to an external magnetic field (Fig. 7.16D).

7.3 Major Applications for the Life Sciences and Environment

Because of their ability to swim in complex fluids, small-scale robots find applications in biomedicine and *on-the-fly chemistry* [3, 14, 94]. In the biomedical area, the community of small-scale robotics is currently working on identifying specific diseases

or conditions where the use of mobile actuatable structures could overcome the challenges of traditional treatments. A clear path in that sense is the use of these motors as drug carriers. While the field of passive nanoparticles delivery still strives in providing an effective solution for the targeted delivery of drugs in affected organs and tissues, the development of controllable micro/nanoscale devices with motile capabilities could revolutionize the directed transportation of therapeutic agents at required body sites. Nevertheless, several challenges accompany the successful translation of small-scale robots to the operating theatre. Perhaps, the most important aspect is to design suitable systems that will enable controlling the motion and actuation of the devices in the intricate architecture of the human body. This is especially noticeable in magnetic small-scale robots. In recent years, we have seen the development of several magnetic navigation systems for maneuvering micro/nanorobots *in vitro* and in vivo. For example, Nelson and co-workers demonstrated the manipulation of swarms of microhelices in the peritoneal cavity of rodents [95]. Yet, the workspace of most of the developed systems cannot accommodate large animals or humans making them unsuitable for translational clinical studies. Magnetic navigation systems compatible with human size such as the AEON Phocus (based on electromagnets) or the Stereotaxis Niobe (based on permanent magnets) have demonstrated the magnetic manipulation of tethered magnetic catheters mainly for endocardial applications [96]. Yet, not all healthcare facilities can adopt such systems considering the required infrastructure and low flexibility (i.e. non-transportable through the hospitals, incompatible with imaging technologies). Additionally, while these systems have demonstrated the manipulation of tethered microcatheters in large animal models, the in vivo manipulation of smaller untethered devices such as micro/nanorobots remains challenging. Other current issues include tracking the devices during their navigation, incorporation of sufficient amounts of therapeutic cargo, biocompatibility, and clearance [124]. In the *on-the-fly chemistry* area [94], most of the concepts that have been reported are limited to the lab scale. While the motion of these devices is useful for accelerating diffusion-limited chemical reactions, the realization of magnetic systems that could actuate micro/nanorobots in large reactors or industrial tanks has not been addressed yet. In the following, we focus on discussing in detail the applications of artificial micro/nanomotors in environmental field, biosensorics, and drug delivery.

7.3.1 Environmental and Bio Remediation

Usage of magnetic micro/nanorobots for environmental remediation is a topic that attracts the enormous attention in the research community. Micromotors hold great promise for environmental remediation, including organic degradation [97, 98], oil extraction [99], and microplastics [100] and heavy metal removal. It was possible to detect and remediate microbial contamination, as well as a general assessment of water quality [100]. Zhang et al. fabricated Au-WO_3@C Janus micromotors with high efficient photocatalytic properties [97] (Fig. 7.17A). Such spherical Janus micromo-

tors display efficient propulsion in pure water with diffusiophoretic effects. WO_3@C Janus micromotors can be accelerated by photocatalytic degradation of dyes such as sodium-2,6-dichloroindophenol and Rhodamine B due to increased diffusiophoretic effects. Dye-induced acceleration offers a promising avenue for using micromotors for environmental applications, ranging from environmental monitoring to environmental remediation. A magnetic layer of Ni can be applied between the Au layer and the WO_3 layer to allow precise control of the motor's motion and facilitate recycling [97]. Vilela et al. reported the use of graphene oxide-based tubular micromotors (GOx-microbots) to capture, transfer, and eliminate a heavy metal (e.g., lead) and to recover it for recycling (Fig. 7.17B) [101]. Microrobots' structure comprises nanosized multilayers of graphene oxide, nickel, and platinum, each providing a different function. Microbots use graphene oxide as the outer layer of the structure to capture lead, platinum as the inner layer to decompose hydrogen peroxide fuel for self-propulsion, and nickel as the middle layer to control the microbots magnetically [101].

Special functionalized micro/nanomotors are useful for target isolation and separation. Guix et al. introduced superhydrophobic alkanethiol-coated Au/Ni/PEDOT/Pt microsubmarines for effective removal of oil (Fig. 7.17C). Oil droplets can be captured, transported, and removed from water samples by highly hydrophobic long-chain alkanethiol monolayers [99].

There is an increased risk of marine life and humans being affected by microplastic (< 5 mm in size), which is not easily sedimented and can pass through filtration systems [100, 102, 103]. Therefore, the development of new methods to reduce the microplastic contamination is one of the critical methods for the whole scientific community. Wang et al. use a photocatalytic TiO_2-based micromotor (Au@mag@TiO_2, mag = Ni, Fe) for microplastic removal (Fig. 7.17D). Namely, this catalytic micromotor can move efficiently and present two novel strategies for the elimination of microplastics based on phoretic interaction. Individual catalytic particles, as well as combined chains, demonstrate excellent elimination of suspended matter and microplastics from environmental water samples [100].

7.3.2 Biosensing

The rich dynamic motion of micro/nanomotors and their responsiveness to the surrounding environment [104] has opened up new opportunities for application in motion-based biosensing and provides an effective motion-based analytical tool for diagnosis [104–107]. The concept of motion-based sensing was first introduced with respect to the detection of silver ions by Wang and co-workers in 2009 [108]. The intrinsic parameters, such as the movement distance, fluorescent turn on/off can be employed directly or indirectly as new analytical signals [109, 110]. Researchers use the speed changes responding to the analytes or the fluorescence quenching methods, to analyze the detection matters with the aid of propelling [107]. Furthermore, the micro/nanomotors can be used to measure the concentration of various

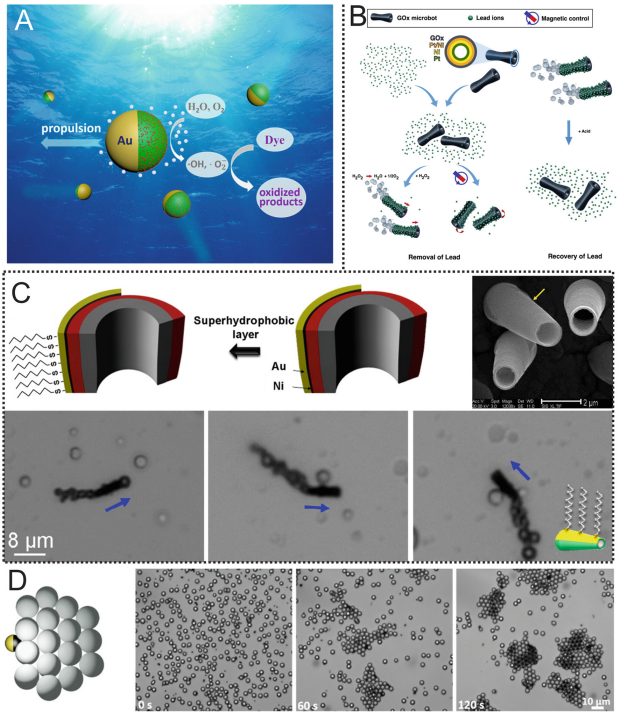

Fig. 7.17 Magnetic micro/nanorobots for environmental remediation. A Au-WO_3@C Janus micromotor shows self-propulsion in low concentrations of sodium-2,6-dichloroindophenol (DCIP) and Rhodamine B (RhB) aqueous solutions, due to the photocatalytic degradation of DCIP and RhB by WO_3. Adapted with permission from [97]. Copyright ©2017 American Chemical Society. **B** The concept for decontaminating and recycling lead using graphene oxide-based tubular micromotors. GOx-microbots fabricated by electrodeposition of nanolayers of graphene oxide, Pt/Ni layer. Graphene oxide nanosheets act as absorption layer due to the strong surface complexation between the Pb (II) ions and the abundant oxygen moieties on the GOx, Ni act as magnetic layer, and Pt act as catalytic inner layer. There are two ways of decontaminating lead ions: by self-propulsion of GOx-microbots in the presence of H_2O_2 or by using an external rotating magnetic field. In the presence of acidic media, lead was recovered from GOx-microbots. Adapted with permission from [101]. Copyright ©2016 American Chemical Society. **C** Superhydrophobic layer is formed on the surface of the Au/Ni/PEDOT/Pt micromotors and used for oil extraction. Time-lapse images showing the Au/Ni/PEDOT/Pt micromotors approaching, contacting, and carrying the droplets, respectively. Inset: Cartoon of the dodecanethiol-modified microsubmarine. Arrows indicate the direction of the micromotor movement. Adapted with permission from [99]. Copyright ©2012 American Chemical Society. **D** Scheme of phoretic interaction between Au@Ni@TiO_2 micromotors and PS particles; time-lapse optical images illustrating Au@Ni@TiO_2 micromotors, collecting PS particles by phoretic interaction in H_2O_2 solution with UV light illumination. Adapted with permission from [100]. Copyright ©2019 American Chemical Society

types of chemicals. Some chemicals like hydrogen peroxide [111], hydrazine [74], and bromine/iodine [112] can be used as fuel for micro/nanomotors. Therefore, a higher concentration of the chemical fuel in the surrounding medium usually leads to a faster-moving speed [104]. Moreover, after surface functionalization, the self-propelled micromotors can capture and transport proteins through selective bounding and show the ability for protein recognition or nucleic acid hybridization [83]. The bound targets were revealed by the detection of fluorescence intensity or speed variation of the micro/nanomotors [106]. The magnetic layer is used to assist in propulsion and motion guidance [113]. Jurado-Sánchez et al. [109] developed a strategy for optical bacterial endotoxins detection. The strategy is based on the use of magnetocatalytic propelled hybrid Janus micromotors (micromotors can actuate in either a catalytic or magnetic mode, catalytically powered by PtNPs or magnetically actuated by Fe_3O_4 NPs) encapsulating highly fluorescent phenylboronic acid (PABA) modified graphene quantum dots (GQDs). In addition to remote magnetic propulsion, Fe_3O_4 nanoparticles provide simultaneous guiding and steering of micromotor under magnetic field. The sensing strategy relies on rapid and specific quenching of fluorescence when GQDs bind with target endotoxin (Fig. 7.18A). Wu et al. [114] present a nanomotor-based biodetection platform for specific DNA and RNA detection. Silver-induced nanomotor speed enhancement was applied for a sensitive, rapid, and simple hybridization assay (Fig. 7.18B). The motion-based hybridization sandwich assay utilizes thiolated DNA capture probes and silver nanoparticle-labeled detection probes (SH-DP-Ag NPs) to form a duplex of nucleic acid targets. The silver nanoparticle labels will dissolve in hydrogen peroxide fuel, which will release silver ions that will make them substantially faster when added to unmodified nanomotor solutions. More silver nanoparticles (AgNPs) will be trapped at higher concentrations of nucleic acids and the nanomotors will have greater velocities. The ferromagnetic nickel segment in the nanomotor can provide a linear distance signal by making this target quantifiable in a convenient and attractive way.

7.3.3 Drug Delivery

Several contributions have been reported in the use of magnetic micro/nanorobots for drug delivery and surgery applications. Yet, most of these studies have been done *in vitro*, and few have been tested using in vivo conditions. Pioneering research in vivo studies with small-scale magnetic motors was realized by Nelson et al. [115]. They first reported the use of magnetic tubular devices for ophthalmologic applications in lapine models [115, 116]. The same group also tested the mobility of a swarm of helical microrobots in the peritoneal cavity of rodents [95].

Zhang and co-workers fabricated helical microrobots with *Spirulina* as templates and navigated them in the stomach of a rat with rotating magnetic fields [117]. The *Spirulina* were coated with magnetite so that they have high responsiveness to external magnetic fields. Compared with the microrobots fabricated using two-photon polymerization, this fabrication method allows for large-scale manufacturing.

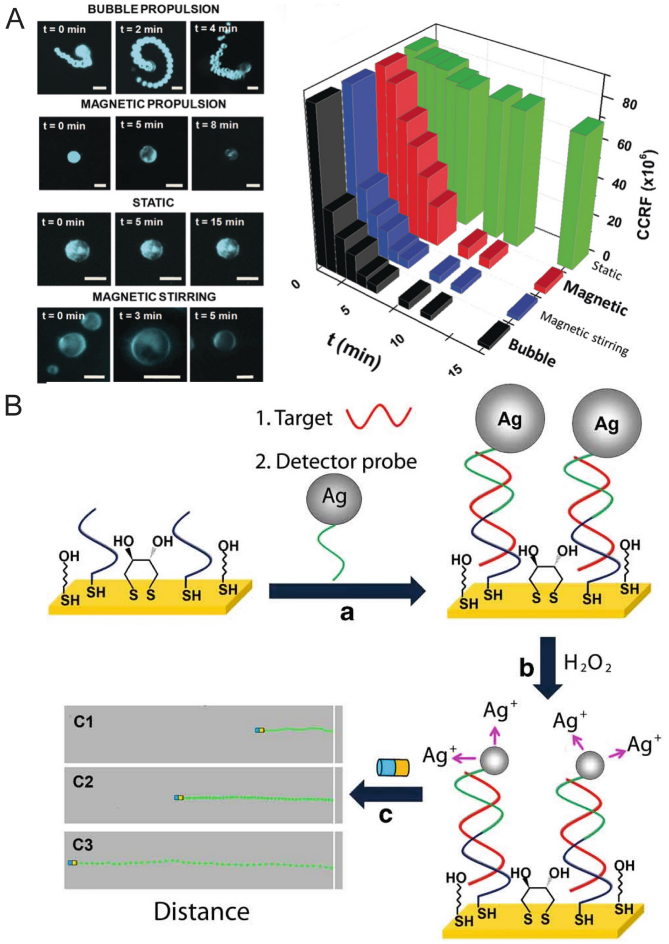

Fig. 7.18 **A** Graphene quantum dots magRobots for the detection of endotoxin from Escherichia coli. Left side is time-lapse microscopy images showing the fluorescence intensity of moving and static micromotors. The right side is corresponding plot showing the fluorescence quenching at different times. Adapted with permission from [109]. Copyright ©2017 Wiley-VCH Verlag GmbH and Co. KGaA, Weinheim. **B** Motion-based nucleic acid detection. First, hybridization of the target and capture of the Ag nanoparticle-tagged detector probe in a typical sandwich assay on the ternary SH-CP/DTT+MCH surface, including washing of unbound SH-DP-Ag NPs. Second, dissolution of silver nanoparticle tags in the peroxide fuel, leading to Ag^{+}-enriched fuel. Then, visual detection of the motion of the Au-Ni-Au-Pt catalytic nanowire motors in the resulting Ag^{+}-enriched fuel. C1, C2, and C3 represent hypothetical and increasing target nucleic acid concentrations. Adapted with permission from [114]. Copyright ©2010, Nature Publishing Group, a division of Macmillan Publishers Limited. All Rights Reserved

The distribution and motion of the microrobots in the body could be tracked by both fluorescence and Magnetic Resonance Imaging (MRI). Besides, magnetite has excellent biocompatible characteristics and can be degraded after the completion of therapeutic tasks [117]. Hybrid microrobots with similar structures were also employed to treat tumors by increasing the O_2 concentration in hypoxic solid tumors for improved effectiveness of radiotherapy in vivo [118]. Apart from *Spirulina*, hybrid microrobots based on cells such as red blood cells, sperm, and neutrophil were also developed for treating different diseases. For example, neutrophil-based magnetic hybrid microrobots have been developed to actively deliver chemodrugs paclitaxel to malignant glioma in vivo [119].

Apart from molecular drugs, therapeutic cells have also been delivered through scaffold-like or porous microrobots. Choi and co-workers developed scaffold-like microrobots using two-photon lithography (the two-photon lithography is described in Chap. 5) and demonstrated that the stem cells could be delivered to the intraperitoneal cavity of a nude mouse [120]. However, these microrobots are still made of negative photoresist, whose biocompatibility is under debate. Porous microrobots made of biodegradable poly(lactic-co-glycolic acid) (PLGA) and iron oxide magnetic nanoparticles were developed for targeted delivery of mesenchymal stem cells close to the defected area for knee cartilage regeneration in vivo. The experimental group with targeted delivery showed an improved cartilage regeneration effect compared with other control groups [121]. Zhang's group developed soft magnetic microrobots directly based on the assembly of stem cells, namely, magnetic stem cell spheroid microrobots (MSCSMs). With endoscopy-assisted magnetic actuation, these microrobots were delivered through the orifice to the bile duct for localized therapy [122].

To achieve the relevant concentration of therapeutics, a swarm of microrobots usually need to be delivered. Zhang and co-workers reported a strategy of navigating a swarm of nanoparticles under ultrasound Doppler imaging guidance for targeted endovascular delivery. The swarm was formed and navigated close to the boundary of the blood vessels, where the blood flow was significantly reduced [123].

Conclusion and Outlook

To conclude, thin magnetic membranes and their curvilinear realizations make very intense contributions to the field of micro/nanorobotics and machinery. After understanding the basic properties and influence of different shapes and geometries on the motion of microscale motors, the scientific community is in an active search of their optimal design and configurations to have a predictable and deterministic motion at the long timescale. The following important milestone will be to reach the level of understanding that will enable the multiple applications of such a type of microsystem. Nowadays, the promising applications of small-scale robots lie in biomedicine and environmental applications and attract more and more scientists to this emerging research field. Here are some considerations before implementing such micro-

objects in real applications. First, micro/nanomotors should meet the requirement to survive in vivo complex environment for biomedicine application and overcome challenges: e.g., minimizing the effect of protein corona, compatible with high ionic strength, surviving the attack from the immune system, and being able to remove from the human body safely or recycle them for later use after the mission is complete. Second, the imaging and real-time precise maneuvering of micro/nanomotors in vivo are very important. Several techniques have been applied to image and track micro/nanomotors in real time, such as magnetic resonance imaging. However, the resolution of current imaging technologies is not high enough to capture individual micro/nanomotors. Wang et al. summarized the multitude of fundamental and practical challenges in translating micro/nanorobots from tabletop studies to clinical applications [124]. Furthermore, it is crucial that micro/nanomotors can coordinate and communicate with each other and perform tasks that a single microrobot cannot. A number of review papers discuss the importance of developing communication and signaling between individual micro/nanorobots. Communicating is essential to designing complex emergent behavior, collective dynamics, and collective intelligence [3, 34, 125].

In summary, interdisciplinary collaboration is essential for the further development and translation of micro/nanorobotic technology into clinical practice. With constant innovation in materials and technologies, we believe relentless efforts will lead us to a new era of micro/nanorobotics.

References

1. F. Peng, Y. Tu, D.A. Wilson, Micro/nanomotors towards in vivo application: cell, tissue and biofluid. Chem. Soc. Rev. **46**(17), 5289–5310 (2017)
2. H. Wang, M. Pumera, Fabrication of micro/nanoscale motors. Chem. Rev. **115**(16), 8704–8735 (2015)
3. F. Soto, E. Karshalev, F. Zhang, B. Esteban Fernandez de Avila, A. Nourhani, J. Wang, Smart materials for microrobots. Chem. Rev. **122**, 5365–5403 (2021)
4. V. Garcia-Gradilla, S. Sattayasamitsathit, F. Soto, F. Kuralay, C. Yardımcı, D. Wiitala, M. Galarnyk, J. Wang, Ultrasound-propelled nanoporous gold wire for efficient drug loading and release. Small **10**(20), 4154–4159 (2014)
5. B.E.F. de Ávila, P. Angsantikul, J. Li, M. Angel Lopez-Ramirez, D.E. Ramírez-Herrera, S. Thamphiwatana, C. Chen, J. Delezuk, R. Samakapiruk, V. Ramez, M. Obonyo, L. Zhang, J. Wang, Micromotor-enabled active drug delivery for in vivo treatment of stomach infection. Nature Commun. **8**(1), 1–9 (2017)
6. S. Wang, X. Liu, Y. Wang, D. Xu, C. Liang, J. Guo, X. Ma, Biocompatibility of artificial micro/nanomotors for use in biomedicine. Nanoscale **11**(30), 14099–14112 (2019)
7. X. Ma, K. Hahn, S. Sanchez, Catalytic mesoporous janus nanomotors for active cargo delivery. J. Am. Chem. Soc. **137**(15), 4976–4979 (2015)
8. C. Peters, M. Hoop, S. Pané, B.J. Nelson, C. Hierold, Degradable magnetic composites for minimally invasive interventions: device fabrication, targeted drug delivery, and cytotoxicity tests. Adv. Mater. **28**(3), 533–538 (2016)
9. H. Xu, M. Medina-Sánchez, V. Magdanz, L. Schwarz, F. Hebenstreit, O.G. Schmidt, Sperm-hybrid micromotor for targeted drug delivery. ACS Nano **12**(1), 327–337 (2018)

10. Z. Wu, X. Lin, X. Zou, J. Sun, Q. He, Biodegradable protein-based rockets for drug transportation and light-triggered release. ACS Appl. Mater. Interfaces **7**(1), 250–255 (2015)
11. S.M. Beladi-Mousavi, B. Khezri, L. Krejčová, Z. Heger, Z. Sofer, A.C. Fisher, M. Pumera, Recoverable bismuth-based microrobots: capture, transport, and on-demand release of heavy metals and an anticancer drug in confined spaces. ACS Appl. Mater. Interfaces **11**(14), 13359–13369 (2019)
12. L. Ren, N. Nama, J.M. McNeill, F. Soto, Z. Yan, W. Liu, W. Wang, J. Wang, T.E. Mallouk, 3D steerable, acoustically powered microswimmers for single-particle manipulation. Sci. Adv. **5**(10), eaax3084 (2019)
13. R.P. Feynman, in *There's Plenty of Room at the Bottom* (Reinhold, New York, 1961), pp. 282–296
14. Z. Wu, Y. Chen, D. Mukasa, O.S. Pak, W. Gao, Medical micro/nanorobots in complex media. Chem. Soc. Rev. **49**(22), 8088–8112 (2020)
15. M. Guix, C.C. Mayorga-Martinez, A. Merkoçi, Nano/micromotors in (bio)chemical science applications. Chem. Rev. **114**(12), 6285–6322 (2014)
16. C. Hu, S. Pané, B.J. Nelson, Soft micro- and nanorobotics. Ann. Rev. Control, Robot. Auton. Syst. **1**(1), 53–75 (2018)
17. W.F. Paxton, K.C. Kistler, C.C. Olmeda, A. Sen, S.K. St. Angelo, Y. Cao, T.E. Mallouk, P.E. Lammert, V.H. Crespi, Catalytic nanomotors: autonomous movement of striped nanorods. J. Am. Chem. Soc. **126**(41) (2004) 13424–13431
18. J. Feng, J. Yuan, S.K. Cho, 2-D steering and propelling of acoustic bubble-powered microswimmers. Lab Chip **16**(12), 2317–2325 (2016)
19. M. Kaynak, A. Ozcelik, A. Nourhani, P.E. Lammert, V.H. Crespi, T.J. Huang, Acoustic actuation of bioinspired microswimmers. Lab Chip **17**(3), 395–400 (2017)
20. O. Dincel, T. Ueta, J. Kameoka, Acoustic driven microbubble motor device. Sens. Actuators, A **295**, 343–347 (2019)
21. A.M. Boymelgreen, T. Balli, T. Miloh, G. Yossifon, Active colloids as mobile microelectrodes for unified label-free selective cargo transport. Nat. Commun. **9**(1), 1–8 (2018)
22. A.F. Demirörs, M.T. Akan, E. Poloni, A.R. Studart, Active cargo transport with janus colloidal shuttles using electric and magnetic fields. Soft Matter **14**(23), 4741–4749 (2018)
23. Y. Wu, A. Fu, G. Yossifon, Active particles as mobile microelectrodes for selective bacteria electroporation and transport. Sci. Adv. **6**(5) (2020)
24. V. Sridhar, B.W. Park, M. Sitti, Light-driven janus hollow mesoporous TiO_2-Au microswimmers. Adv. Func. Mater. **28**(25), 1704902 (2018)
25. R. Dong, Y. Cai, Y. Yang, W. Gao, B. Ren, Photocatalytic micro/nanomotors: From construction to applications. Acc. Chem. Res. **51**(9), 1940–1947 (2018)
26. Z. Wu, X. Lin, Y. Wu, T. Si, J. Sun, Q. He, Near-infrared light-triggered "on/offâŁž motion of polymer multilayer rockets. ACS Nano **8**(6), 6097–6105 (2014)
27. Y. Zong, J. Liu, R. Liu, H. Guo, M. Yang, Z. Li, K. Chen, An optically driven bistable janus rotor with patterned metal coatings. ACS Nano **9**(11), 10844–10851 (2015)
28. K.E. Peyer, S. Tottori, F. Qiu, L. Zhang, B.J. Nelson, Magnetic helical micromachines. Chem. Eur. J. **19**(1), 28–38 (2013)
29. A.M. Maier, C. Weig, P. Oswald, E. Frey, P. Fischer, T. Liedl, Magnetic propulsion of microswimmers with DNA-based flagellar bundles. Nano Lett. **16**(2), 906–910 (2016)
30. H. Xu, M. Medina-Sánchez, O.G. Schmidt, Magnetic micromotors for multiple motile sperm cells capture, transport, and enzymatic release. Angew. Chem. **132**(35), 15139–15147 (2020)
31. H. Zhou, C.C. Mayorga-Martinez, S. Pané, L. Zhang, M. Pumera, Magnetically driven micro and nanorobots. Chem. Rev. **121**(8), 4999–5041 (2021)
32. L. Ren, W. Wang, T.E. Mallouk, Two forces are better than one: combining chemical and acoustic propulsion for enhanced micromotor functionality. Acc. Chem. Res. **51**(9), 1948–1956 (2018)
33. C. Chen, S. Tang, H. Teymourian, E. Karshalev, F. Zhang, J. Li, F. Mou, Y. Liang, J. Guan, J. Wang, Chemical/light-powered hybrid micromotors with "on-the-fly" optical brakes. Angewandte Chemie Int. Ed. **57**(27), 8110–8114 (2018)

34. H. Wang, M. Pumera, Coordinated behaviors of artificial micro/nanomachines: from mutual interactions to interactions with the environment. Chem. Soc. Rev. **49**(10), 3211–3230 (2020)
35. J. Wang, *Nanomachines: Fundamentals and Applications* (Wiley, New York, 2013)
36. D. Pantarotto, W.R. Browne, B.L. Feringa, Autonomous propulsion of carbon nanotubes powered by a multienzyme ensemble. Chem. Commun. **13**, 1533–1535 (2008)
37. D. Xu, C. Zhou, C. Zhan, Y. Wang, Y. You, X. Pan, J. Jiao, R. Zhang, Z. Dong, W. Wang, X. Ma, Enzymatic micromotors: Enzymatic micromotors as a mobile photosensitizer platform for highly efficient on-chip targeted antibacteria photodynamic therapy (adv. funct. mater. 17/2019). Adv. Funct. Mater. **29**(17), 1970112 (2019)
38. X. Chen, C. Zhou, W. Wang, Colloidal motors 101: a beginner's guide to colloidal motor research. Chem. Asian J. **14**(14), 2388–2405 (2019)
39. L. Ricotti, B. Trimmer, A.W. Feinberg, R. Raman, K.K. Parker, R. Bashir, M. Sitti, S. Martel, P. Dario, A. Menciassi, Biohybrid actuators for robotics: a review of devices actuated by living cells. Sci. Robot. **2**(12) (2017)
40. L. Baraban, R. Streubel, D. Makarov, L. Han, D. Karnaushenko, O.G. Schmidt, G. Cuniberti, Fuel-free locomotion of janus motors: magnetically induced thermophoresis. ACS Nano **7**(2), 1360–1367 (2013)
41. L. Baraban, D. Makarov, R. Streubel, I. Mönch, D. Grimm, S. Sanchez, O.G. Schmidt, Catalytic janus motors on microfluidic chip: deterministic motion for targeted cargo delivery. ACS Nano **6**(4), 3383–3389 (2012)
42. T.R. Kline, W.F. Paxton, T.E. Mallouk, A. Sen, Catalytic nanomotors: remote-controlled autonomous movement of striped metallic nanorods. Angew. Chem. Int. Ed. **44**(5), 744–746 (2005)
43. T. Li, J. Li, H. Zhang, X. Chang, W. Song, Y. Hu, G. Shao, E. Sandraz, G. Zhang, L. Li, J. Wang, Magnetically propelled fish-like nanoswimmers. Small **12**(44), 6098–6105 (2016)
44. W. Gao, X. Feng, A. Pei, C.R. Kane, R. Tam, C. Hennessy, J. Wang, Bioinspired helical microswimmers based on vascular plants. Nano Lett. **14**(1), 305–310 (2014)
45. L.O. Mair, B.A. Evans, A. Nacev, P.Y. Stepanov, R. Hilaman, S. Chowdhury, S. Jafari, W. Wang, B. Shapiro, I.N. Weinberg, Magnetic microkayaks: propulsion of microrods precessing near a surface by kilohertz frequency, rotating magnetic fields. Nanoscale **9**(10), 3375–3381 (2017)
46. A.A. Solovev, S. Sanchez, M. Pumera, Y.F. Mei, O.G. Schmidt, Magnetic control of tubular catalytic microbots for the transport, assembly, and delivery of micro-objects. Adv. Func. Mater. **20**(15), 2430–2435 (2010)
47. Y. Mei, A.A. Solovev, S. Sanchez, O.G. Schmidt, Rolled-up nanotech on polymers: from basic perception to self-propelled catalytic microengines. Chem. Soc. Rev. **40**(5), 2109 (2011)
48. F. Mushtaq, A. Asani, M. Hoop, X.Z. Chen, D. Ahmed, B.J. Nelson, S. Pané, Highly efficient coaxial TiO_2-PtPd tubular nanomachines for photocatalytic water purification with multiple locomotion strategies. Adv. Func. Mater. **26**(38), 6995–7002 (2016)
49. K. Yuan, V. de la Asunción-Nadal, B. Jurado-Sánchez, A. Escarpa, 2D nanomaterials wrapped janus micromotors with built-in multiengines for bubble, magnetic, and light driven propulsion. Chem. Mater. **32**(5), 1983–1992 (2020)
50. L. Zhang, J.J. Abbott, L. Dong, K.E. Peyer, B.E. Kratochvil, H. Zhang, C. Bergeles, B.J. Nelson, Characterizing the swimming properties of artificial bacterial flagella. Nano Lett. **9**(10), 3663–3667 (2009)
51. E.J. Smith, D. Makarov, S. Sanchez, V.M. Fomin, O.G. Schmidt, Magnetic microhelix coil structures. Phys. Rev. Lett. **107**(9), 097204 (2011)
52. M.A. Zeeshan, S. Pané, S.K. Youn, E. Pellicer, S. Schuerle, J. Sort, S. Fusco, A.M. Lindo, H.G. Park, B.J. Nelson, Graphite coating of iron nanowires for nanorobotic applications: Synthesis, characterization and magnetic wireless manipulation. Adv. Func. Mater. **23**(7), 823–831 (2013)
53. L. Zhang, T. Petit, Y. Lu, B.E. Kratochvil, K.E. Peyer, R. Pei, J. Lou, B.J. Nelson, Controlled propulsion and cargo transport of rotating nickel nanowires near a patterned solid surface. ACS Nano **4**(10), 6228–6234 (2010)

54. A. Ghosh, P. Fischer, Controlled propulsion of artificial magnetic nanostructured propellers. Nano Lett. **9**(6), 2243–2245 (2009)
55. L. Zhang, J.J. Abbott, L. Dong, B.E. Kratochvil, D. Bell, B.J. Nelson, Artificial bacterial flagella: fabrication and magnetic control. Appl. Phys. Lett. **94**(6), 064107 (2009)
56. X.Z. Chen, M. Hoop, F. Mushtaq, E. Siringil, C. Hu, B.J. Nelson, S. Pané, Recent developments in magnetically driven micro- and nanorobots. Appl. Mater. Today **9**, 37–48 (2017)
57. D. Yamamoto, A. Shioi, Self-propelled nano/micromotors with a chemical reaction: underlying physics and strategies of motion control. Kona Powder Part. J. **32**, 2–22 (2015)
58. W. Wang, W. Duan, S. Ahmed, T.E. Mallouk, A. Sen, Small power: autonomous nano- and micromotors propelled by self-generated gradients. Nano Today **8**(5), 531–554 (2013)
59. J. Li, B. Esteban-Fernández de ávila, W. Gao, L. Zhang, J. Wang, Micro/nanorobots for biomedicine: delivery, surgery, sensing, and detoxification. Sci. Robot. **2**(4), eaam6431 (2017)
60. E.M. Purcell, Life at low reynolds number. Am. J. Phys. **45**(1), 3–11 (1977)
61. K.E. Peyer, L. Zhang, B.J. Nelson, Bio-inspired magnetic swimming microrobots for biomedical applications. Nanoscale **5**(4), 1259–1272 (2013)
62. C. Pauer, O. du Roure, J. Heuvingh, T. Liedl, J. Tavacoli, Programmable design and performance of modular magnetic microswimmers. Adv. Mater. **33**(16), 2006237 (2021)
63. J.R. Howse, R.A.L. Jones, A.J. Ryan, T. Gough, R. Vafabakhsh, R. Golestanian, Self-motile colloidal particles: from directed propulsion to random walk. Phys. Rev. Lett. **99**(4), 048102 (2007)
64. X.Z. Chen, N. Shamsudhin, M. Hoop, R. Pieters, E. Siringil, M.S. Sakar, B.J. Nelson, S. Pané, Magnetoelectric micromachines with wirelessly controlled navigation and functionality. Mater. Horiz. **3**(2), 113–118 (2016)
65. Z. Ye, M. Sitti, Dynamic trapping and two-dimensional transport of swimming microorganisms using a rotating magnetic microrobot. Lab Chip **14**(13), 2177–2182 (2014)
66. T.O. Tasci, P.S. Herson, K.B. Neeves, D.W.M. Marr, Surface-enabled propulsion and control of colloidal microwheels. Nat. Commun. **7**(1), 1–6 (2016)
67. C.E. Sing, L. Schmid, M.F. Schneider, T. Franke, A. Alexander-Katz, Controlled surface-induced flows from the motion of self-assembled colloidal walkers. Proc. Natl. Acad. Sci. **107**(2), 535–540 (2010)
68. T. Li, A. Zhang, G. Shao, M. Wei, B. Guo, G. Zhang, L. Li, W. Wang, Janus microdimer surface walkers propelled by oscillating magnetic fields. Adv. Func. Mater. **28**(25), 1706066 (2018)
69. I.S.M. Khalil, V. Magdanz, S. Sanchez, O.G. Schmidt, S. Misra, Precise localization and control of catalytic janus micromotors using weak magnetic fields. Int. J. Adv. Rob. Syst. **12**(1), 2 (2015)
70. H. Ye, Y. Wang, X. Liu, D. Xu, H. Yuan, H. Sun, S. Wang, X. Ma, Magnetically steerable iron oxides-manganese dioxide core-shell micromotors for organic and microplastic removals. J. Colloid Interface Sci. **588**, 510–521 (2021)
71. M. Vilfan, A. Potočnik, B. Kavčič, N. Osterman, I. Poberaj, A. Vilfan, D. Babič, Self-assembled artificial cilia. Proc. Natl. Acad. Sci. **107**(5), 1844–1847 (2010)
72. B. Jang, A. Hong, C. Alcantara, G. Chatzipirpiridis, X. Martí, E. Pellicer, J. Sort, Y. Harduf, Y. Or, B.J. Nelson, S. Pané, Programmable locomotion mechanisms of nanowires with semihard magnetic properties near a surface boundary. ACS Appl. Mater. Interfaces **11**(3), 3214–3223 (2019)
73. A.A. Solovev, Y. Mei, E. Bermúdez Ureña, G. Huang, O.G. Schmidt, Catalytic microtubular jet engines self-propelled by accumulated gas bubbles. Small **5**(14), 1688–1692 (2009)
74. Y. Mei, G. Huang, A.A. Solovev, E. Bermúdez Ureña, I. Mönch, F. Ding, T. Reindl, R.K.Y. Fu, P.K. Chu, O.G. Schmidt, Versatile approach for integrative and functionalized tubes by strain engineering of nanomembranes on polymers. Adv. Mater. **20**(21), 4085–4090 (2008)
75. O.G. Schmidt, K. Eberl, Thin solid films roll up into nanotubes. Nature **410**(6825), 168–168 (2001)
76. K.M. Manesh, M. Cardona, R. Yuan, M. Clark, D. Kagan, S. Balasubramanian, J. Wang, Template-assisted fabrication of salt-independent catalytic tubular microengines. ACS Nano **4**(4), 1799–1804 (2010)

77. W. Gao, S. Sattayasamitsathit, J. Orozco, J. Wang, Highly efficient catalytic microengines: template electrosynthesis of polyaniline/platinum microtubes. J. Am. Chem. Soc. **133**(31), 11862–11864 (2011)
78. Z. Wu, Y. Wu, W. He, X. Lin, J. Sun, Q. He, Self-propelled polymer-based multilayer nanorockets for transportation and drug release. Angew. Chem. Int. Ed. **52**(27), 7000–7003 (2013)
79. F. Qiu, B.J. Nelson, Magnetic helical micro- and nanorobots: Toward their biomedical applications. Engineering **1**(1), 021–026 (2015)
80. T. Xu, G. Hwang, N. Andreff, S. Régnier, The rotational propulsion characteristics of scaled-up helical microswimmers with different heads and magnetic positioning, in *2013 IEEE/ASME International Conference on Advanced Intelligent Mechatronics* (IEEE, 2013), pp 1114–1120
81. G. Chatzipirpiridis, C. de Marco, E. Pellicer, O. Ergeneman, J. Sort, B.J. Nelson, S. Pané, Template-assisted electroforming of fully semi-hard-magnetic helical microactuators. Adv. Eng. Mater. **20**(9), 1800179 (2018)
82. A.M. Leshansky, K.I. Morozov, B.Y. Rubinstein, Shape-controlled anisotropy of superparamagnetic micro-/nanohelices. Nanoscale **8**(29), 14127–14138 (2016)
83. J. Kim, S.E. Chung, S.E. Choi, H. Lee, J. Kim, S. Kwon, Programming magnetic anisotropy in polymeric microactuators. Nat. Mater. **10**(10), 747–752 (2011)
84. C. Peters, O. Ergeneman, P.D.W. García, M. Müller, S. Pané, B.J. Nelson, C. Hierold, Superparamagnetic twist-type actuators with shape-independent magnetic properties and surface functionalization for advanced biomedical applications. Adv. Func. Mater. **24**(33), 5269–5276 (2014)
85. S. Gervasoni, A. Terzopoulou, C. Franco, A. Veciana, N. Pedrini, J.T. Burri, C. de Marco, E.C. Siringil, X. Chen, B.J. Nelson, J. Puigmartí-Luis, S. Pané, CANDYBOTS: A new generation of 3D-printed sugar-based transient small-scale robots. Adv. Mater. **32**(52), 2005652 (2020)
86. H.W. Huang, F.E. Uslu, P. Katsamba, E. Lauga, M.S. Sakar, B.J. Nelson, Adaptive locomotion of artificial microswimmers. Sci. Adv. **5**(1), eaau1532 (2019)
87. S. Fusco, H.W. Huang, K.E. Peyer, C. Peters, M. Häberli, A. Ulbers, A. Spyrogianni, E. Pellicer, J. Sort, S.E. Pratsinis, B.J. Nelson, M.S. Sakar, S. Pané, Shape-switching microrobots for medical applications: the influence of shape in drug delivery and locomotion. ACS Appl. Mater. Interfaces **7**(12), 6803–6811 (2015)
88. S. Fusco, M.S. Sakar, S. Kennedy, C. Peters, R. Bottani, F. Starsich, A. Mao, G.A. Sotiriou, S. Pané, S.E. Pratsinis, D. Mooney, B.J. Nelson, An integrated microrobotic platform for on-demand, targeted therapeutic interventions. Adv. Mater. **26**(6), 952–957 (2014)
89. Q. Chen, P. Lv, J. Huang, T.Y. Huang, H. Duan, Intelligent shape-morphing micromachines. Research **2021**, 1–16 (2021)
90. H.W. Huang, M.S. Sakar, A.J. Petruska, S. Pané, B.J. Nelson, Soft micromachines with programmable motility and morphology. Nat. Commun. **7**(1), 1–10 (2016)
91. W. Hu, G.Z. Lum, M. Mastrangeli, M. Sitti, Small-scale soft-bodied robot with multimodal locomotion. Nature **554**(7690), 81–85 (2018)
92. J. Cui, T.Y. Huang, Z. Luo, P. Testa, H. Gu, X.Z. Chen, B.J. Nelson, L.J. Heyderman, Nanomagnetic encoding of shape-morphing micromachines. Nature **575**(7781), 164–168 (2019)
93. Y. Alapan, A.C. Karacakol, S.N. Guzelhan, I. Isik, M. Sitti, Reprogrammable shape morphing of magnetic soft machines. Sci. Adv. **6**(38), eabc6414 (2020)
94. E. Karshalev, B. Esteban-Fernández de Ávila, J. Wang, Micromotors for "chemistry-on-the-fly". J. Am. Chem. Soc. **140**(11), 3810–3820 (2018)
95. A. Servant, F. Qiu, M. Mazza, K. Kostarelos, B.J. Nelson, Controlled in vivo swimming of a swarm of bacteria-like microrobotic flagella. Adv. Mater. **27**(19), 2981–2988 (2015)
96. F. Carpi, C. Pappone, Stereotaxis niobe® magnetic navigation system for endocardial catheter ablation and gastrointestinal capsule endoscopy. Expert Rev. Med. Devices **6**(5), 487–498 (2009)
97. Q. Zhang, R. Dong, Y. Wu, W. Gao, Z. He, B. Ren, Light-driven Au-WO_3@C janus micromotors for rapid photodegradation of dye pollutants. ACS Appl. Mater. Interfaces **9**(5), 4674–4683 (2017)

98. F. Mushtaq, M. Guerrero, M.S. Sakar, M. Hoop, A.M. Lindo, J. Sort, X. Chen, B.J. Nelson, E. Pellicer, S. Pané, Magnetically driven Bi_2O_3/BiOCl-based hybrid microrobots for photocatalytic water remediation. J. Mater. Chem. A **3**(47), 23670–23676 (2015)
99. M. Guix, J. Orozco, M. García, W. Gao, S. Sattayasamitsathit, A. Merkoçi, A. Escarpa, J. Wang, Superhydrophobic alkanethiol-coated microsubmarines for effective removal of oil. ACS Nano **6**(5), 4445–4451 (2012)
100. L. Wang, A. Kaeppler, D. Fischer, J. Simmchen, Photocatalytic TiO_2 micromotors for removal of microplastics and suspended matter. ACS Appl. Mater. Interfaces **11**(36), 32937–32944 (2019)
101. D. Vilela, J. Parmar, Y. Zeng, Y. Zhao, S. Sánchez, Graphene-based microbots for toxic heavy metal removal and recovery from water. Nano Lett. **16**(4), 2860–2866 (2016)
102. A.L. Andrady, Microplastics in the marine environment. Mar. Pollut. Bull. **62**(8), 1596–1605 (2011)
103. S.E. Nelms, J. Barnett, A. Brownlow, N. Davison, R. Deaville, T.S. Galloway, P.K. Lindeque, D. Santillo, B.J. Godley, Microplastics in marine mammals stranded around the british coast: ubiquitous but transitory? Sci. Rep. **9**(1), 1–8 (2019)
104. K. Kim, J. Guo, Z. Liang, D. Fan, Artificial micro/nanomachines for bioapplications: Biochemical delivery and diagnostic sensing. Adv. Func. Mater. **28**(25), 1705867 (2018)
105. H. Wang, M.G. Potroz, J.A. Jackman, B. Khezri, T. Marić, N.J. Cho, M. Pumera, Bioinspired spiky micromotors based on sporopollenin exine capsules. Adv. Func. Mater. **27**(32), 1702338 (2017)
106. L. Kong, J. Guan, M. Pumera, Micro- and nanorobots based sensing and biosensing. Curr. Opin. Electrochem. **10**, 174–182 (2018)
107. H. Ye, Y. Wang, D. Xu, X. Liu, S. Liu, X. Ma, Design and fabrication of micro/nano-motors for environmental and sensing applications. Appl. Mater. Today **23**, 101007 (2021)
108. D. Kagan, P. Calvo-Marzal, S. Balasubramanian, S. Sattayasamitsathit, K.M. Manesh, G.U. Flechsig, J. Wang, Chemical sensing based on catalytic nanomotors: motion-based detection of trace silver. J. Am. Chem. Soc. **131**(34), 12082–12083 (2009)
109. B. Jurado-Sánchez, M. Pacheco, J. Rojo, A. Escarpa, Magnetocatalytic graphene quantum dots janus micromotors for bacterial endotoxin detection. Angew. Chem. Int. Ed. **56**(24), 6957–6961 (2017)
110. Y. Zhang, L. Zhang, L. Yang, C.I. Vong, K.F. Chan, W.K.K. Wu, T.N.Y. Kwong, N.W.S. Lo, M. Ip, S.H. Wong, J.J.Y. Sung, P.W.Y. Chiu, L. Zhang, Real-time tracking of fluorescent magnetic spore-based microrobots for remote detection of C. diff toxins. Sci. Adv. **5**(1), eaau9650 (2019)
111. H. Wang, G. Zhao, M. Pumera, Beyond platinum: Bubble-propelled micromotors based on Ag and MnO_2 catalysts. J. Am. Chem. Soc. **136**(7), 2719–2722 (2014)
112. R. Liu, A. Sen, Autonomous nanomotor based on copper-platinum segmented nanobattery. J. Am. Chem. Soc. **133**(50), 20064–20067 (2011)
113. M. Koleoso, X. Feng, Y. Xue, Q. Li, T. Munshi, X. Chen, Micro/nanoscale magnetic robots for biomedical applications. Materials Today Bio **8**, 100085 (2020)
114. J. Wu, S. Balasubramanian, D. Kagan, K.M. Manesh, S. Campuzano, J. Wang, Motion-based DNA detection using catalytic nanomotors. Nat. Commun. **1**(1), 1–6 (2010)
115. G. Chatzipirpiridis, O. Ergeneman, J. Pokki, F. Ullrich, S. Fusco, J.A. Ortega, K.M. Sivaraman, B.J. Nelson, S. Pané, Electroforming of implantable tubular magnetic microrobots for wireless ophthalmologic applications. Adv. Healthcare Mater. **4**(2), 209–214 (2015)
116. F. Ullrich, S. Fusco, G. Chatzipirpiridis, S. Pané, B.J. Nelson, Recent progress in magnetically actuated microrobotics for ophthalmic therapies. Europ. Ophthalm. Rev. **08**(02), 120 (2014)
117. X. Yan, Q. Zhou, M. Vincent, Y. Deng, J. Yu, J. Xu, T. Xu, T. Tang, L. Bian, Y.X.J. Wang, K. Kostarelos, L. Zhang, Multifunctional biohybrid magnetite microrobots for imaging-guided therapy. Sci. Robot. **2**(12), eaaq1155 (2017)
118. D. Zhong, W. Li, Y. Qi, J. He, M. Zhou, Photosynthetic biohybrid nanoswimmers system to alleviate tumor hypoxia for FL/PA/MR imaging-guided enhanced radio-photodynamic synergetic therapy. Adv. Func. Mater. **30**(17), 1910395 (2020)

119. H. Zhang, Z. Li, C. Gao, X. Fan, Y. Pang, T. Li, Z. Wu, H. Xie, Q. He, Dual-responsive biohybrid neutrobots for active target delivery. Sci. Robot. **6**(52), eaaz9519 (2021)
120. S. Jeon, S. Kim, S. Ha, S. Lee, E. Kim, S.Y. Kim, S.H., Park, J.H., Jeon, S.W. Kim, C. Moon, B.J. Nelson, J.Y. Kim, S.W. Yu, H. Choi, Magnetically actuated microrobots as a platform for stem cell transplantation. Sci. Robot. **4**(30), eaav4317 (2019)
121. G. Go, S.G. Jeong, A. Yoo, J. Han, B. Kang, S. Kim, K.T. Nguyen, Z. Jin, C.S. Kim, Y.R. Seo, J.Y. Kang, J.Y., Na, E.K Song, Y. Jeong, J.K. Seon, J.O. Park, E. Choi, Human adipose-derived mesenchymal stem cell-based medical microrobot system for knee cartilage regeneration in vivo. Sci. Robot. **5**(38), eaay6626 (2020)
122. B. Wang, K.F. Chan, K. Yuan, Q Wang, X. Xia, L. Yang, H. Ko, Y.X.J. Wang, J.J.Y. Sung, P.W.Y. Chiu, L. Zhang, Endoscopy-assisted magnetic navigation of biohybrid soft microrobots with rapid endoluminal delivery and imaging. Sci. Robot. **6**(52) eabd2813 (2021)
123. Q. Wang, K.F. Chan, K. Schweizer, X. Du, D. Jin, S.C.H. Yu, B.J. Nelson, L. Zhang, Ultrasound doppler-guided real-time navigation of a magnetic microswarm for active endovascular delivery. Sci. Adv. **7**(9), eabe5914 (2021)
124. W. Wang, C. Zhou, A journey of nanomotors for targeted cancer therapy: principles, challenges, and a critical review of the state-of-the-art. Adv. Healthcare Mater. **10**(2), 2001236 (2021)
125. L. Huang, J.L. Moran, W. Wang, Designing chemical micromotors that communicate-a survey of experiments. JCIS Open **2**, 100006 (2021)